ACS APPLIED BIO MATERIALS

www.acsabm.org

Article

Innate Immune Mechanisms Triggered by SARS-CoV-2 Virus-Like Particles: Role of Antibody Opsonization

Asta Lučiūnaitė,* Mantvydas Usvaltas, Vincentas Maciulis, and Ieva Plikusiene*

Cite This: *ACS Appl. Bio Mater.* 2026, 9, 5196−5215

Read Online

ACCESS | Metrics & More | Article Recommendations | Supporting Information

ABSTRACT: The rapid spread of SARS-CoV-2 highlighted the need to understand the nature of innate immune signaling. We used virus-like particles (VLPs) composed of SARS-CoV-2 structural proteins, spike, envelope, membrane, and nucleocapsid, mimicking the virus to study macrophage responses to VLPs and their immune complexes (ICs), which represent antibody-opsonized particles cleared by innate immune cells. We assessed antibody affinity and IC properties using quartz crystal microbalance with dissipation (QCM-D). Human THP-1-derived macrophages treated with VLPs or ICs showed inflammatory activation, including inflammasome signaling, chemokine receptor expression, and antigen-presentation-related markers CD86/CD83. Notably, ICs triggered lower chemokine secretion but similar TNF-α release and enhanced IL-1β production, with increased ASC protein expression in some cases. These findings reveal distinct macrophage responses to viral antigens vs ICs, emphasizing IC-driven inflammasome activation during SARS- CoV-2 infection, independent of chemokine secretion profiles.

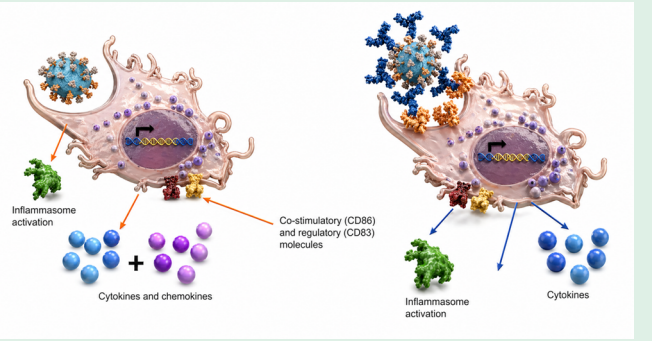

KEYWORDS: *antibody, viral antigen, immune complex, biosensing, macrophage*

INTRODUCTION

The COVID-19 pandemic raised several questions related to understanding the innate antiviral immune response. Innate immune cells, such as macrophages, are the first to encounter pathogens and are responsible for removing viral antigens opsonized by antibodies that are produced during the humoral immune response.[1] Antibody-opsonized antigens, called ICs, also mediate effector functions in macrophages.[2,3] These cells can induce a strong inflammatory response that sometimes leads to hyperinflammation and tissue damage. This issue was noticed in some cases of SARS-CoV-2 infection.[4] It has been shown that monocytes/macrophages significantly contribute to hyperinflammation by secreting substantial amounts of inflammatory cytokines, including chemokines that recruit other immune cells.[5] Moreover, inflammasome activation was observed during strong inflammatory conditions. ICs, formed by the SARS-CoV-2 virus, can activate the inflammasome, which was confirmed experimentally. Antibody-opsonized SARS-CoV-2 particles can even enhance the inflammatory response in circulating monocytes by mediating the inflammasome activation,[6] and the virus itself can activate the inflammasome in monocytes[7] and macrophages,[8] worsening the infection. Hyperinflammation caused by IC-triggered inflammasome activation was also demonstrated in other viral infections, such as the dengue virus.[9] Antibody-dependent enhancement, characterized by an inflammatory response mediated by antibody-opsonized viruses in Fc receptor (FcR)-positive immune cells, has been documented in various viral infections, including respiratory syncytial virus,[10,11] measles,[12] and SARS-CoV-2.[13,14] The severity of viral disease can also be correlated with antibody titer, as well as hyperinflammation. For example, in the case of COVID-19, accumulated inflammatory macrophages play a crucial role during inflammation.[5] Furthermore, antibodies can enhance virus entry into the cell through FcR, leading to increased virus production, as demonstrated with infectious diseases caused by the dengue virus[15,16] and coronaviruses.[17,18] This phenomenon of cell infection through the entry of a virion into an immune cell by receptor-mediated endocytosis has been known for many years.[19] However, the additional cell activation mechanisms might vary between viruses, and they have not been sufficiently investigated. Intracellular signals induced by the entered virions might be potential defence mechanisms to reduce virus production. For example, in lung macrophages, the inflammasome is activated

Received: February 23, 2026
Revised: May 6, 2026
Accepted: May 7, 2026
Published: May 26, 2026

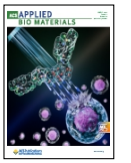

https://doi.org/10.1021/acsabm.6c00372
ACS Appl. Bio Mater. 2026, 9, 5196−5215

by the SARS-CoV-2 virion, followed by pyroptosis to prevent virus production within the cells.[8] As a result, lung hyperinflammation is induced, but the spread of infection is also blocked. Previously, we demonstrated that antibodies could enhance viral antigen-mediated inflammasome activation in murine macrophages.[20] Additionally, our results showed that IC properties shape the IC-induced inflammatory response. We used a multivalent antigen model derived from the major capsid protein VP1 of the nonenveloped polyomavirus that mimics the structure of the viral particle. Comprehensive characterization of our ICs revealed that ICs differed according to the antibody affinity to the antigen and relative size, as described by the number of antibodies covering the antigen. We demonstrated the importance of antibody properties in IC-mediated innate immune cell activation.

In some cases, SARS-CoV-2 infection develops into hyperinflammation and immunopathology.[4,21] In severe SARS-CoV-2 infection, the IC role is also highlighted by high levels of virus-specific IgG in circulation, together with ICs and excessive FcγRIIIA activation found in the patients.[22] Interestingly, the concentration of soluble ICs in circulation correlates with the severity of the disease. Recent studies have focused on the factors influencing these immunopathological effects. Some of them showed that glycosylation, such as fucosylation of the antibody's Fc fragment may be a determining factor in different abilities to cope with infection and further development of various pathologies.[13,23,24] Antibody-dependent enhancement was shown to be tightly related to antibody fucosylation.[25,26] In SARS-CoV-2, afucosylated antibodies were described as inflammation-driving factors that enhance formed IC interaction with activating FcRs, followed by increased production of inflammatory cytokines, which correlates with infection severity.[13] Overall, the experimental and clinical data highlight ICs as the main players in a severe SARS-CoV-2 infection.

Different IC interactions with FcRs may be determined not only by antibody Fc fragment glycosylation, which influences antibody affinity for FcR, but also by the properties of the formed IC. IC interaction with FcRs mediates cellular signals that induce specific antibody effector functions, such as the production of inflammatory molecules and reactive oxygen species, as well as the upregulation of FcR for IC phagocytosis.[27] Inflammatory chemokines can recruit other immune cells to the site of infection and enhance inflammatory reactions.[28] However, detailed signaling pathways of macrophage activation by ICs are not sufficiently elucidated. Therefore, investigations on viral antigens and their IC-induced cellular effector functions are crucial for a deeper understanding of the antiviral innate immune response, which can influence the further development of hyperinflammation and even tissue damage leading to fibrosis. It is known that to transduce cell activation signals, cross-linking of antibodies opsonizing antigens is required.[29−31] This highlights the significance of the properties of multivalent ICs on cellular response. It is also known that, in addition to post-translation modifications of the Fc fragment, antibody affinity and IC size can influence IC interaction with FcRs, which leads to signal transduction.[32−35] Moreover, it was demonstrated that antibodies binding to the receptor-binding domain of the SARS-CoV-2 spike protein can exacerbate FcR-mediated enhancement of virus infection.[36] Bioinformatic analysis of antibodies specific to the receptor-binding domain of the SARS-CoV-2 spike protein demonstrated that antibody affinity and epitope have a high impact on antibody-mediated effector functions.[37] Antibodies are prominent tools for antiviral therapy;[38] however, we still do not fully understand the IC-mediated cell activation mechanisms and the impact of antibody properties on this process. Therefore, treatment with antiviral antibodies can have unexpected consequences, such as antibody-mediated enhancement or hyperinflammation.[39] Understanding of cell activation mechanisms induced by IC would provide the ability to modulate macrophage responses in certain viral infections or antibody therapies, thus avoiding adverse reactions.

In this study, we investigated the interactions between innate immune cells, macrophages, and multivalent viral antigens and their formed multivalent ICs. We applied SARS-CoV-2 VLPs derived from virus structural proteins (spike, nucleocapsid, membrane, and envelope), mimicking the native viral structure. This multimeric protein complex has many antibody-binding sites; thus, it forms multivalent ICs like viral particles in body circulation. To form ICs, we applied different monoclonal antibody models, including the natural human IgG1 antibody CR3022 and several llama nanobodies (VHH) fused with human IgG1 Fc (VHH-Fc). To investigate the cell activation profile induced by a multivalent viral antigen and innate immune cell effector functions mediated by an antibody-opsonized antigen, we assessed the chemokine secretion profile, inflammatory signals, including inflammasome activation and the production of inflammatory molecules, as well as the surface expression of molecules related to antigen presentation and chemokine receptors. The interaction of VLP with antibody models was measured simultaneously using highly sensitive and label-free acoustic and optical methods, such as quartz crystal microbalance with dissipation (QCM-D) and spectroscopic ellipsometry (SE).[40] QCM-D measures changes in frequency (proportional to surface mass) and energy dissipation (relative to viscoelasticity), and SE measures the refractive index of polarized light upon sample surface reflection that is relative to the thickness of the layer. However, the SE method did not evaluate the appropriate signal of VLPs; therefore, only QCM-D measurements were used. QCM-D data demonstrated real-time IC formation between VLPs and various monoclonal antibody models, while calculated interaction kinetics revealed a high affinity of all antibodies. Cell activation analysis demonstrated that both VLPs and ICs induced inflammatory responses, including inflammasome activation, in macrophages. Interestingly, antibody-opsonized VLPs did not mediate inflammatory chemokine secretion, contrary to VLPs alone. We also found that VLPs and their ICs induced the expression of antigen presentation-related molecules CD83 and CD86 on the surface of the macrophage. CD86 is expressed in macrophages of an inflammatory phenotype[41] while CD83 is a regulatory molecule related to the resolution of inflammation.[42] Overall, our data show that SARS-CoV-2 VLPs mediate a complex macrophage activation profile, and their opsonization with antibodies did not reduce inflammatory signals but influenced the chemokine secretion profile.

METHODS

Materials

Human antibodies anti-spike (S) protein in PBS with 0.02% Proclin 300, Cstock = 1.0 mg/ml (Absolute Antibodies), clones: Anti-COVID-19 & SARS-CoV S glycoprotein #CR3022 (cat# Ab01680-10.0); Human IgG1-Fc Fusion Anti-Spike protein (RBD) Sb#14

https://doi.org/10.1021/acsabm.6c00372
ACS Appl. Bio Mater. 2026, 9, 5196−5215

(cat# Ab02012-10.159), Sb#15 (cat#Ab02013-10.159), and Sb#68 (cat# Ab02017-10.159); CR3022—natural human IgG1 antibody, Sb14, Sb15, and Sb68—VHH-Fc of IgG1 fusion antibodies. 40 nm size SARS-CoV-2 spike WT virus-like-particles (VLPs) of four structural proteins: Membrane (M), Nucleocapsid (N), Spike (S), and Envelope (E), produced in HEK293 cells, C_{stock} = 1.0 mg/ml, in 10 mM Tris, 1 M NaCl, pH 7.4 (20% sucrose, 1 mM EDTA, cat#P6677) were purchased from Abnova. Recombinant SARS-CoV-2 WT spike protein-full-length trimeric ectodomain, C_{stock} = 1.0 mg/ml (cat# 20-S2S-TCg-F) was obtained from Baltymas. Cell culture medium Roswell Park Memorial Institute (RPMI) 1640 + GlutaMAX (cat#61870044), 1% penicillin/streptomycin solution (PSI, cat#15140122), and fetal bovine serum (FBS; cat# A3840402) were purchased from Gibco, Thermo Fisher Scientific. LDH assay: Cytotoxicity Detection Kit PLUS (LDH), cat#4744934001, was obtained from CYTODET-RO Roche, Merck. Phorbol 12-myristate-13-acetate (PMA, cat# P1585-1MG) was purchased from Sigma-Aldrich by Merck. Live Cell Imaging Solution (cat#A14291DJ) and Hoechst 33342 10 mg/ml (cat#H3570) were purchased from Invitrogen, Thermo Fisher Scientific. 11-Mercaptoundecanoic acid (11-MUA, 98%), 1-ethyl-3-(3-dimethylaminopropyl) carbodiimide (EDC, ≥98%), *N*-hydroxysuccinimide (NHS, 98%), and ethanolamine (ETA) (≥99%) were purchased from Sigma Aldrich. Methanol (99.9%), hydrochloric acid (37%), and glycine (≥99%) were purchased from Carl Roth GmbH & Co (Karlsruhe, Germany). Gold-coated QCM−D quartz crystals with a resonance frequency of 4.95 MHz and a diameter of 14 mm were purchased from Biolin Scientific (Gothenburg, Sweden).

Cell Culture

THP-1 and THP-1-ASC-GFP monocytic cell lines were used to prepare macrophages. THP-1 was kindly given by Dr. Linas Mažutis lab (Life Sciences Center, Vilnius University), purchased from ATCC (cat#TIB-202). THP-1-ASC-GFP was purchased from InvivoGen (cat#thp-ascgfp). Cells were cultivated in RPMI 1640 medium supplemented with 1/1% penicillin/streptomycin and 10% heat-inactivated serum (serum medium). For cultivating THP-1-ASC-GFP, antibiotics normocin and zeocin were used additionally. Cells were differentiated to macrophage-like cells using phorbol 12-myristate 13-acetate (PMA, cat# P1585-1MG, Sigma-Aldrich by Merck). 100 ng/mL PMA was added for 48 h, and then it was replaced with fresh serum medium for a 24 h resting period. Differentiated cells were used for the analysis. The cells were treated with serum-free RPMI 1640 medium supplemented with penicillin/streptomycin. Cells were activated with 15 μg/ml viral antigens (~83.3 nM of VLPs or spike protein, considering 180 kDa molar mass of spike protein) and different ICs for 24 h. ICs were formed from ~83.3 nM antigens and 27.7 nM antibody models (M_w of CR3022 is 150 kDa, M_w of Sb14, Sb15, and Sb68 is 75 kDa, according to the manufacturer) by incubating for 30 min at 37 °C. After cell treatment, cell culture supernatants were collected for evaluation of cytokine secretion, and the cells were used for flow cytometry analysis. The cells were seeded in 24 well cell culture plates (cat#92024, cell culture-treated surface, TPP), at a density of 0.125 million cells per well. For microscopy analysis, cells were seeded in a black square-96-well plate (cat#89626 Ibi-treat, Ibidi), at a density of 0.08 million cells per well. Live cells were used for the analysis.

Chemokine Secretion Determined by Proteomic Chemokine Array

To determine the chemokine secretion profile, the Proteome Profiler Human Chemokine Array Kit (cat#ARY017, R&D Systems) was applied. All procedures were performed according to the manufacturer's protocol. The kit is based on Western blot analysis and contains 4 membranes. Each membrane was used for different treatment conditions (spike protein, VLPs, ICs of VLPs and Sb14, and ICs of VLPs and Sb68). For each treatment condition, a mixture of supernatants of 5 independent cell culture preparations was used. Undiluted supernatants were used for the array. The membranes with samples were incubated overnight. The blots were developed using the ChemiDoc Imaging System (Bio-Rad Laboratories). The spots on the blots were quantified using ImageJ with the Protein Array Analyzer open-source plugin, developed by Gilles Carpentier. The spot intensity was calculated as integrated area values and was used for further analysis with Python. Spots of Negative Control (referred to by the manufacturer) were used to extract the background from the calculated spot intensity signal. Each chemokine had two repeats in the array. The average values were used in heatmaps, bubble plots, and volcano plots to calculate fold changes between different treatments. For the volcano plot, p-values were calculated using a *t*-test from two repeats.

Secretion of Cytokines by Enzyme-Linked Immunosorbent Assay (ELISA)

To detect the secretion of cytokines (including chemokines), their concentration was measured in collected cell culture supernatants by ELISA. The following ELISA kits were used: Human IL-1 beta Uncoated ELISA Kit (cat#88-7261-86) and Human TNF alpha Uncoated ELISA Kit (cat#88-7346-86) were purchased from Invitrogen, Thermo Fisher Scientific; Human IL-8/CXCL8 ELISA Development Kit (TMB, cat #900-T18K) was obtained from PeproTech, Thermo Fisher Scientific; and Human CCL5/RANTES DuoSet ELISA kit (cat#DY278), Human CXCL10/IP-10 DuoSet ELISA kit (cat#DY266), Human CCL3/MIP-1 alpha DuoSet ELISA kit (cat#DY270), and Human CCL4/MIP-1 beta DuoSet ELISA kit (cat#DY271) were obtained from R&D Systems. The assay was performed according to the manufacturer's protocols.

Cellular Activation Marker Expression by Flow Cytometry

Expression of CCR2, CCR5, CD83, and CD86 was measured by the flow cytometry method. After the treatment, the cells were washed with ice-cold PBS/EDTA (cat#9152.1, CellPure, Carl Roth). Fresh PBS/EDTA was then added, and the cells were detached from the growing surface using cell scrapers, all while keeping them on ice. After centrifugation at 300 × g for 10 min, cells were resuspended in a 2% BSA solution in PBS with Fc block (1:50) and an unlabeled IgG2b mouse isotype control (for CCR5 staining, as the antibody specific to CCR5 is of the mouse IgG2b subtype), and incubated for 15 min. The antibodies were added directly to the blocking solution (1:100) and incubated for 30 min. Respective isotype controls were added to a mix of all samples. After a 30-min incubation with antibodies, 7-AAD cell viability dye was added for 5 min. Cells were centrifuged at 300 × g for 5 min and then resuspended in a PBS/EDTA solution. The fluorescent signal was measured by BD FACS Symphony A1 flow cytometry. The data were analyzed by FlowJo analysis software. Duplets (according to FSC-A and FSC-H gating) and dead cells (7-AAD positive) were excluded from the analysis. The area parameter of fluorescent intensity was used for the analysis. The fraction of marker-positive cells (%) and mean fluorescent intensity (MFI) were calculated.

Human TruStain FcX (Fc Receptor Blocking Solution, cat#422302) was from Biolegend. Flow cytometry antibodies against human antigens: anti-CD86-AlexaFluor 488 (cat#53-0869-42, clone B7-2, Invitrogen, Thermo Fischer Scientific), anti-CCR2-PE (cat#357206, clone K036C2, Biolegend), anti-CD83-AlexaFluor 647 (cat#305316, clone HB15e, Biolegend), anti-CCR5-AlexaFluor 405 (cat#FAB184V-100UG, Clone #45529, R&D Systems). Isotype controls: Unstained Mouse IgG2b Isotype Control (cat#MAB004, Clone # 20116, R&D Systems); PE Mouse IgG2a, κ Isotype Ctrl clone MOPC-173 (cat# 400214, Biolegend); Mouse IgG2b kappa Isotype Control (eBMG2b) Alexa Fluor 488, eBioscience (Cat# 53-4732-80, Invitrogen, Thermo Fischer Scientific); and Alexa Fluor 647 Mouse IgG1, κ Isotype Ctrl (cat#400130, Biolegend).

https://doi.org/10.1021/acsabm.6c00372
ACS Appl. Bio Mater. 2026, 9, 5196−5215

Microscopy Analysis

ASC speck formation and ASC protein expression in THP-1-ASC-GFP macrophages were measured using a wide-field, fully automated microscope Nikon Eclipse Ti-2E. An objective lens with a 20× magnification was used. 10 photos per well were taken. The object counts and MFI analysis were performed with the Nikon NIS-Element analysis program. Data were processed with Python. 30 min before the treatment, Hoechst 33342 nuclear stain was added to visualize the cell nucleus and used for cell counting. Propidium iodide (PI) nuclear stain was used to visualize dead cells. Live cells were examined in Live Cell Imaging solution.

SE/QCM-D Measurement Configuration

Ellipsometric and QCM-D measurements were performed simultaneously to enable real-time monitoring of interfacial processes. SE was carried out using a rotating compensator ellipsometer (M-2000X, J. A. Woollam, Lincoln, NE, USA) at a fixed angle of incidence of 65° over a spectral range of 200–1000 nm. The ellipsometric parameters delta (Δ) and psi (Ψ) were continuously recorded and evaluated using the proprietary CompleteEASE software (version 6.73gsc). QCM-D measurements of frequency (ΔF) and dissipation (ΔD) were conducted using a QSense Explorer (Biolin Scientific, Västra Frölunda, Sweden) operating at a fundamental frequency of 5 MHz and capable of simultaneously registering seven harmonics up to approximately 65 MHz. The measurements were performed using a specialized module designed for simultaneous SE and QCM-D acquisition of signal, allowing complementary optical and acoustic characterization of surface-bound layers in situ. QCM-D data were recorded with QSoft401 and analyzed using QSense Dfind software, while additional mathematical processing was carried out in Origin. Fluid handling was controlled by an Ismatec IPC4 peristaltic pump (Cole-Palmer GmbH, Wertheim, Germany) connected to the measurement cell via PTFE tubing. All measurements were performed under semi-static conditions with a flow rate of 1 mL/min, and the temperature was maintained at 20 °C.

QCM-D Sensor Surface Functionalization

The QCM-D sensor discs were cleaned by immersion in deionized water and methanol for 5 min each in an ultrasonic bath. After cleaning, the sensors were immersed in a 1 mM solution of 11-MUA in methanol for 18 h to form a self-assembled monolayer (SAM) presenting terminal carboxyl groups. Following SAM formation, the sensors were air-dried to remove residual solvent and mounted in the QCM-D measurement module. The chamber was filled with PBS to hydrate the surface and establish a stable baseline. The carboxyl groups of the 11-MUA SAM were activated by injecting a freshly prepared solution of 0.1 M NHS and 0.4 M EDC, mixed in equal volumes, for 15 min. This activation step enabled the covalent immobilization of biomolecules onto the functionalized sensor surface.

Antibody–Antigen Interaction Measurements by Combined SE and QCM-D

Antibody–antigen interactions were measured by monitoring the VLP interaction with affinity-immobilized antibody models. Protein G was covalently immobilized on activated SAM. An antibody solution at a concentration of 200 nM was affinity-immobilized on Protein G, followed by injection of the antigen at a concentration of 100 nM into the measurement chamber. Real-time kinetics of antibody–antigen interactions were measured for up to 1 h. Surface regeneration was performed using 10 mM glycine-hydrochloride solution (pH 2.0). Measurements were performed using a simultaneous combination of two methods—QCM-D and SE. Real-time changes in frequencies and dissipation (QCM-D), refractive index, and thickness of the formed protein layers (SE) were obtained. Mathematical models were applied to quantify kinetic parameters, such as rate and affinity constants. QCM-D parameters: changes in frequency and dissipation were used to evaluate the surface mass density and to determine IC layer viscoelasticity, which is related to conformational changes during macromolecule interactions. QCM-D gave information on the surface mass density of the buffer and macromolecules of the formed IC, while SE—on the dry protein mass.

Statistical Analysis

Data were processed and evaluated using GraphPad Prism 10.6.1 software and the Python programming language, based on at least 5 independent experiments. Statistical comparisons of controls vs treatment were analyzed with one-way ANOVA. If the data did not pass the normality test, the Kruskal–Wallis test with Dunn's post-hoc test was applied. Statistically significant results are referred to as $^{*}P < 0.05$, $^{**}P < 0.01$, $^{***}P < 0.001$, $^{****}P < 0.0001$. The data are represented by bar graphs with individual data points showing mean with standard deviation or by violin plots showing minimum and maximum values, median, first and third quartiles, also in truncated violin plots without minimum and maximum values for better visualization.

RESULTS

To investigate the influence of antibody properties on their formed ICs and further induced macrophage effector functions, we used natural human IgG1 antibody CR3022 and VHH-Fc IgG1 fusion proteins (VHH-Fc). The CR3022 antibody sequence was extracted from an antibody naturally circulating in the human body after SARS-CoV-2 infection. We selected three VHH-Fc antibodies specific to the receptor-binding domain of the SARS-CoV-2 spike protein (Sb14, Sb15, and Sb68), which may form different ICs. As an antigen model, we used recombinant VLPs of SARS-CoV-2 structural proteins—spike, envelope, nucleocapsid, and membrane proteins. This allowed for the use of multivalent ICs mimicking antigens opsonized by antibodies found in body circulation. The use of different antibody models extended our research to the characterization of VHH-Fc applications, not only as an immunoassay tool but also for their possible implementation in medicine. To describe the antibody–VLP interaction, we applied the advanced biosensing-based technique QCM-D. From the measurements, we calculated the kinetic parameters of the antibody–VLP interaction and the affinity constants of the antibody. QCM-D parameter dissipation was used to characterize the viscoelasticity of the formed IC layer, which is associated with conformational changes during protein–protein interactions. Another QCM-D parameter change in frequency was used to characterize the surface mass density, including protein and buffer molecules. These characteristics were used to determine the influence of IC properties on induced inflammatory responses, describing effector functions in macrophages.

Characterization of Antibody–Antigen Interactions

The antibody–VLP interaction was simultaneously measured by SE and QCM-D. VLPs' binding kinetics were measured on affinity-immobilized antibody models via protein G. We got a very small signal from SE measurements compared to QCM-D (calculated SE parameter Γ^{SE} over time of antibody-VLP interaction, Figure 1). Therefore, we considered this optical method to be unsuitable for VLP signal detection. The antibody-VLP interaction analysis was performed using QCM-D data. VLPs showed high affinity for all investigated antibody models, with the highest K_D value observed for Sb14 (K_D, Table 1), although all affinity constants K_D were of the same order (10^{-10}). The rate constant of stable IC layer

https://doi.org/10.1021/acsabm.6c00372
ACS Appl. Bio Mater. 2026, 9, 5196–5215

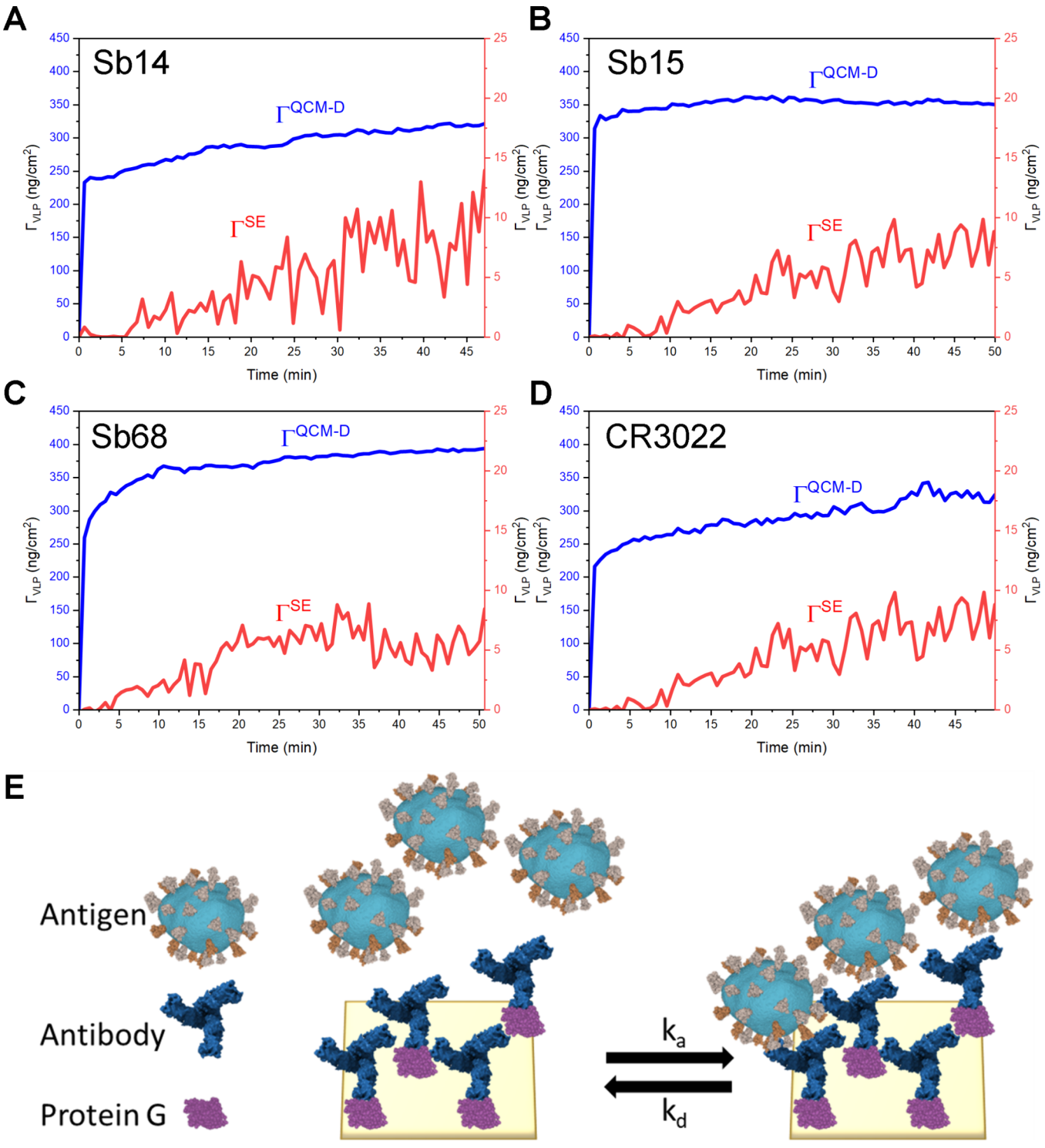

Figure 1. Real-time characterization of antibody–VLP interaction by QCM-D and SE. Antibodies were affinity immobilized via protein G. IC layer formation was described by different surface mass density parameters $\Gamma^{QCM\text{-}D}$ and Γ^{SE} for different antibody models: (A) Sb14, (B) Sb15, (C) Sb68, and (D) CR3022. The curves show changes in VLP surface mass density over time. (E) Schematic representation of antibody interaction with VLPs, rate constants for association (k_a), and dissociation (k_d).

formation showed that the VLPs formed complexes with Sb14 faster than with the other VHH-Fcs, whereas complex formation with Sb68 was the slowest (k_r, Table 1). The rate constant for stable VLP−CR3022 complex formation indicated exceptionally slow IC formation, on the order of 10^{-17}.

The QCM-D frequency shift (ΔF) was used to calculate the antibody mass, which includes the hydrodynamically coupled buffer, using the Sauerbrey equation. The overall IC mass was calculated using the Voinova–Voight model (calculated mass $\Gamma^{QCM\text{-}D}$; Figure 1, Table 2). To determine the surface mass

https://doi.org/10.1021/acsabm.6c00372
ACS Appl. Bio Mater. 2026, 9, 5196−5215

Table 1. Kinetics of Antibody–VLP Interactions from QCM-D Data[a]

sample	k_a ($M^{-1}s^{-1}$)	k_r (s^{-1})	k_d (s^{-1})	K_A (M^{-1})	K_D (m)	ΔG (kJ/mol)
SB14/VLP	9.47×10^4	1.04×10^{-5}	1.63×10^{-5}	5.81×10^9	1.72×10^{-10}	−54.8
SB15/VLP	8.68×10^4	1.15×10^{-5}	3.34×10^{-5}	2.60×10^9	3.85×10^{-10}	−52.8
SB68/VLP	4.90×10^4	9.31×10^{-6}	1.55×10^{-5}	3.16×10^9	3.16×10^{-10}	−53.3
CR3022/VLP	2.19×10^5	2.50×10^{-17}	9.1×10^{-5}	2.38×10^9	4.21×10^{-10}	−52.6

[a]Rate constants for association (k_a) and dissociation (k_d), stable IC formation (k_r); K_A—association constant, K_D—dissociation/affinity constant, ΔG—change in Gibbs free energy during VLP association with immobilized antibody models.

Table 2. Characteristics of Antibody–VLP Layer Formation: Surface Mass Density (Γ^{SE}, $\Gamma^{QCM\text{-}D}$), Change in Frequency (ΔF), and Change in Dissipation (ΔD) over Time during IC Formation[a]

interaction	VLP $\Gamma^{QCM\text{-}D}$, ng/cm^2	Ab $\Gamma^{QCM\text{-}D}$, ng/cm^2	Ab Γ^{SE}, ng/cm^2	ab f_{PBS}, %	ΔF, Hz, 3rd harmonic	ΔD, $\times 10^{-6}$, 3rd harmonic
SB14/VLP	321.9	568.9	223.6	60.7	3.93	1.5
SB15/VLP	350.5	539.0	223.1	58.6	4.12	1.44
SB68/VLP	394.3	576.8	202.2	64.9	8.35	1.97
CR3022/VLP	324.4	791.7	306.9	61.2	3.15	1.47

[a]Ab—antibody.

density from SE measurements, an optical model was constructed and fitted to the measured ellipsometric parameters Ψ and Δ. The SE data were analyzed in the CompleteEASE software by regression analysis of the optical model. As separate VLP layer properties were hard to extract, the ICs were modeled as a single layer consisting of CR3022 or VHH-Fcs with attached VLP. From the fitted model, the refractive index and thickness of the formed layers were obtained. These parameters were then used to calculate the surface mass density using the de Feijter formula[40] (eq 1):

$$\Gamma = \frac{d(n_{layer} - n_{buffer})}{\Delta n/\Delta c} \times 100 \quad (1)$$

where $\Delta n/\Delta c$ is the refractive index increment which links the refractive index of the layer to the concentration of protein in the solution and is equal to 0.18 cm^3/g,[43] d is the thickness of the layer (nm), n_{layer} is the refractive index of the layer obtained from the optical model, and n_{buffer} is the refractive index of the buffer solution. Effective layer thicknesses of ICs obtained from the SE optical model were used to determine the size of ICs by summing the thickness of the antibody layer and the VLP layer. Using this approach, the largest estimated IC size was observed for CR3022−VLP (48.3 nm), whereas SB14−VLP, SB15−VLP, and SB68−VLP exhibited smaller values of 37.1, 42.18, and 43.5 nm, respectively. Relatively, the highest mass was associated with the formation of the Sb68−VLP IC. Real-time IC formation, measured by QCM-D, showed dynamic interactions between different antibody models and antigens. The dissipation parameter D was used to evaluate the surface rigidity of the formed antibody−VLP layer. High ΔD values demonstrated the formation of a highly viscoelastic layer, indicating continuous conformational changes (Table 2). Comparing all antibody models, Sb68 distinguishes itself by the slowest formation of a stable antibody−VLP complex among the VHH-Fc constructs. At the same time, Sb68 formed the largest IC layer, possibly the highest amount of VLPs attached to the VHH-Fc surface compared to other antibody models, with the surface mass density reaching 394.3 ng/cm^2 ($\Gamma^{QCM\text{-}D}$, Table 2).

To evaluate possible conformational changes during antibody binding to the antigen, $\Delta D/\Delta F$ plots were made by showing time on a color scale (Figure 2). If there are no intensive dynamic processes during biomolecular interactions, ΔD scales linearly with ΔF, and the slope remains approximately constant in a $\Delta D/\Delta F$ plot. During conformational changes of interacting biomolecules, the energy loss occurs, and it is described by ΔD parameter linearity deviations, which are reflected by changes in slope in the $\Delta D/\Delta F$ plot.[44] Firstly, we analyzed side-directed immobilization of different antibody models via affinity interaction with covalently immobilized protein G. Oriented antibody immobilization resulted in a highly rigid and compact surface layer, consistent with dense antibody packing (scatter plots, Figure 2A−D). Comparing all antibody models, Sb68 distinguished itself from other VHH-Fcs (Figure 2C) by exhibiting distinct conformational changes during binding to protein G, taking the longest to reach the maximum dissipation at approximately 240 s. After reaching the maximum, all studied antibody models showed a linear decrease in dissipation. On the contrary, the Sb68 monolayer exhibited additional conformational rearrangements at approximately 1545 s, after which a linear increase in ΔD was observed. Interestingly, all VHH-Fcs had the same IgG1 Fc fragment. We also observed intensive conformational changes during antibody−VLP layer formation, as indicated by the non-linear ΔD/ΔF plots with several steps (Figure 2E−H). Sb14−VLP, Sb15−VLP, and Sb68−VLP IC formation each proceeded in two distinct steps. Compared to the other ICs, Sb68−VLP complex formation suggested different conformational changes during VLP binding to Sb68, as reflected by the slowest increase in dissipation and a maximum ΔD reached at approximately 360 s. Excluding the third overtone, ΔD remained elevated until the maximum frequency shift was attained. The $\Delta D/\Delta F$ plot of the CR3022−VLP interaction also had 2 steps, but the form of the plot was completely different from other ICs (Figure 2H). The formation of the CR3022−VLP complex reached the maximum ΔD more rapidly, at approximately 70 s. This was followed by a linear decrease in both dissipation and ΔF shift, indicating that a stable complex was not formed. This antibody is approximately twice the size of the VHH-Fc antibody models and has a

https://doi.org/10.1021/acsabm.6c00372
ACS Appl. Bio Mater. 2026, 9, 5196−5215

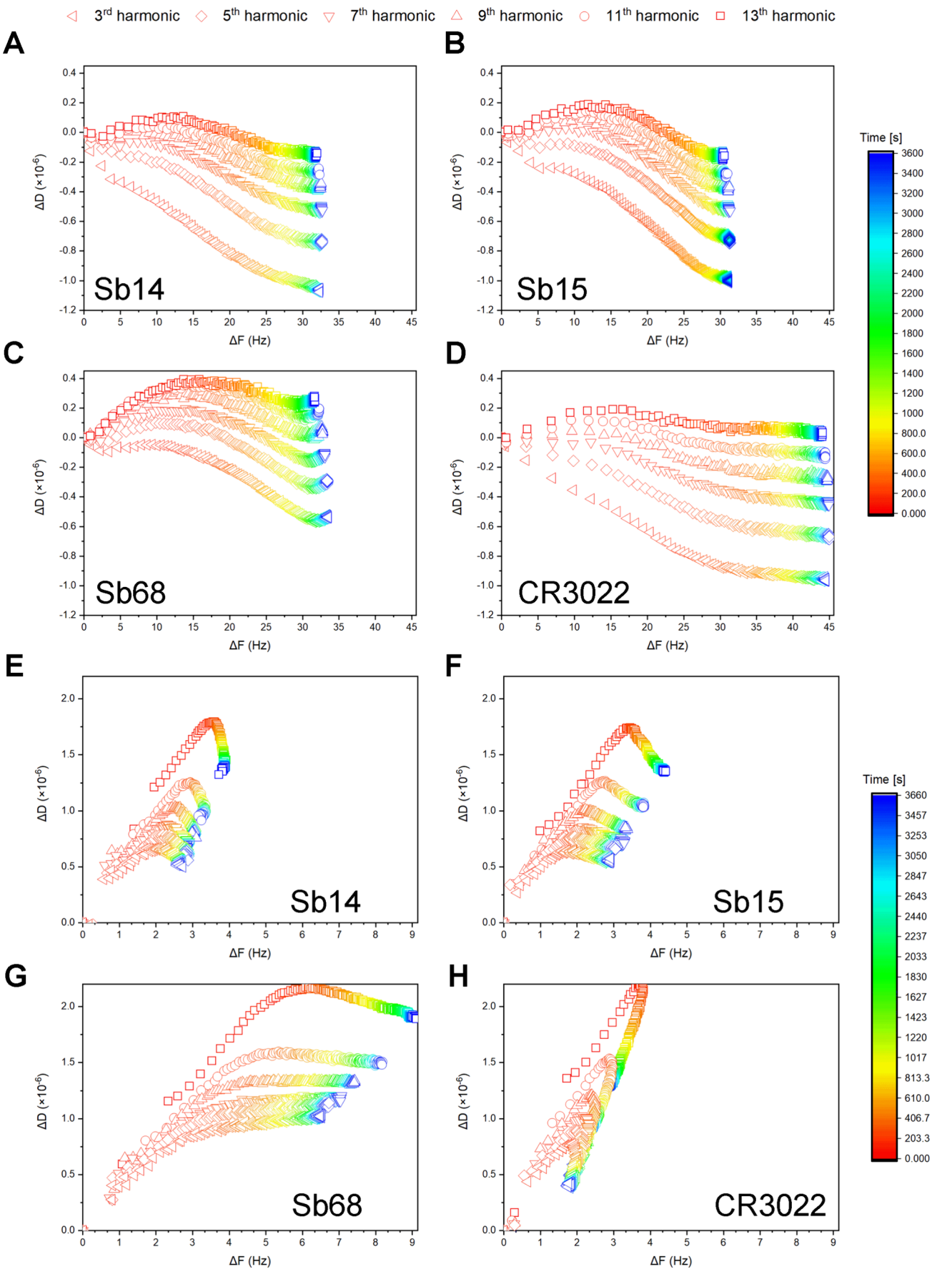

https://doi.org/10.1021/acsabm.6c00372
ACS Appl. Bio Mater. 2026, 9, 5196−5215

Figure 2. continued

ΔD vs ΔF plots of antibody–VLP interaction. $\Delta D/\Delta F$ plots were obtained by plotting ΔF on the *x*-axis and ΔD on the *y*-axis and the color scales indicate the elapsed time of antibody affinity immobilization via interaction with protein G for different antibody models: (A) Sb14, (B) Sb15, (C) Sb68, and (D) CR3022. $\Delta D/\Delta F$ plots for VLPs binding to affinity immobilized antibody surfaces: (E) Sb14, (F) Sb15, (G) Sb68, and (H) CR3022. Different harmonics of oscillating quartz crystal with formed layers are shown, probing different sensing depths relative to the sensor surface.

completely different Fab fragment, which could lead to different antigen binding dynamics.

Evaluation of VLP Cytotoxicity

Cell viability and metabolic activity were measured using the LDH detection assay. VLPs and their ICs induced up to 8 times higher release of LDH compared to control treatments (untreated cell control value, 0, and no antibody (Ab) is 100%, Figure 3). This was equal to the positive control, which shows the total amount of LDH released by dead cells (Triton X-100, Figure 3). However, after cell staining with dead cell nucleus stain propidium iodide, only a few dead cells were found (Figure 3C). As the LDH amount also indicates cell metabolic activity, these results revealed that VLPs and their ICs induced a slight increase in cell death and an enormous increase in macrophage metabolic activity.

INFLAMMASOME ACTIVATION PROFILE INDUCED BY VLPS AND ICS IN MACROPHAGES

We measured inflammasome activation by evaluating inflammasome priming, IL-1β release, cell death, and apoptosis-associated speck-like protein containing a CARD (ASC) speck formation. Cell death induced by VLPs and their ICs was shown by the release of LDH and staining with propidium iodide (Figure 3). By measuring the expression of ASC protein induced by activation of the NF-dB pathway, we found that both VLPs and ICs mediated the priming of inflammasome

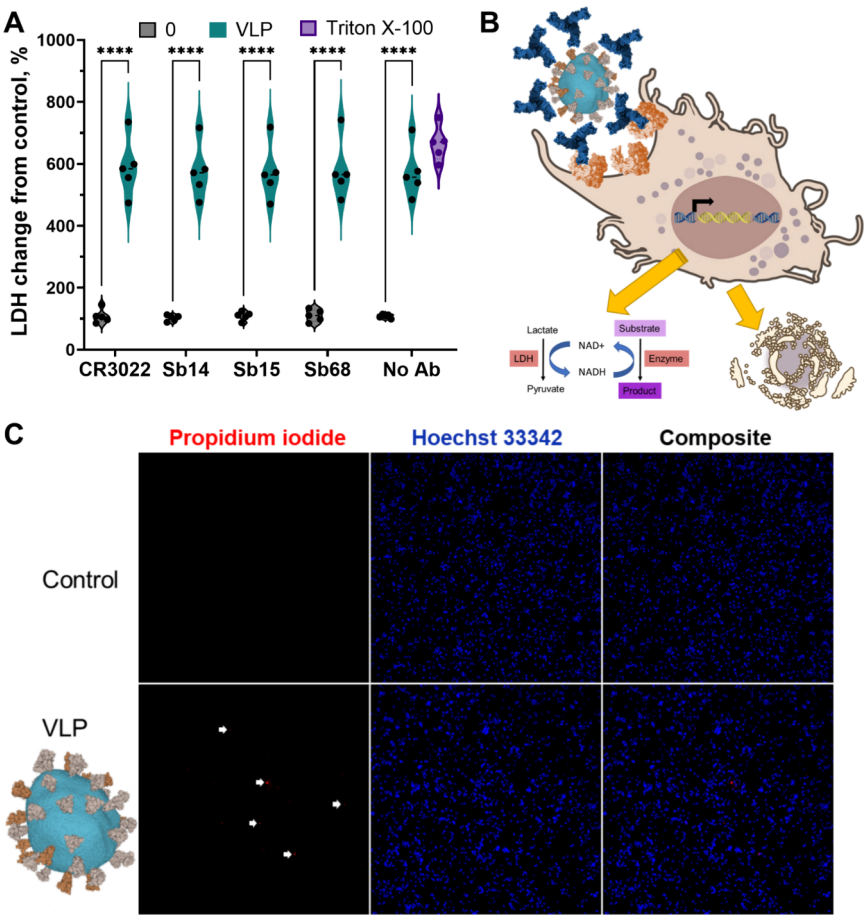

Figure 3. Cytotoxicity and metabolic activity induced by VLPs and their ICs in THP-1 macrophages. Cells were treated for 24 h with VLPs and their ICs or respective controls. Triton X-100 was used as a positive control. LDH level was measured in collected cell culture supernatant to assess metabolic activity and cell death. Live cells were stained with propidium iodide and analyzed by microscopy to evaluate cell death. (A) LDH released expressed as a change from untreated cell control (value equals 100%, 0, and no antibody (Ab)). (B) Illustrating image of cell treatment and LDH assay showing cell death and metabolic activity. (C) Representative image of propidium iodide (dead cells) and Hoechst33342 (all cells) nuclear staining. White arrows show dead cells. Data are presented in violin plots with individual data points, $N = 5$ independent cell culture preparations. A two-way ANOVA with Šídák's multiple comparisons test was used, $^{****}P < 0.0001$.

https://doi.org/10.1021/acsabm.6c00372
ACS Appl. Bio Mater. 2026, 9, 5196−5215

activation (Figure 4). As a protein control, we used pure SARS-CoV-2 spike protein. We haven't detected any effect of spike protein on the inflammatory signal (Figure 4). The inflammasome priming effect by VLPs was also confirmed by the increased release of the inflammatory cytokine TNF-α (Figure 4). Both VLPs and ICs mediated IL-1β secretion, ASC speck formation (Figure 4), and cell death (Figure 3), showing inflammasome activation. Comparing VLPs and ICs, we haven't detected significant differences in TNF-α secretion (Figure 4), but we found higher secretion of IL-1β induced

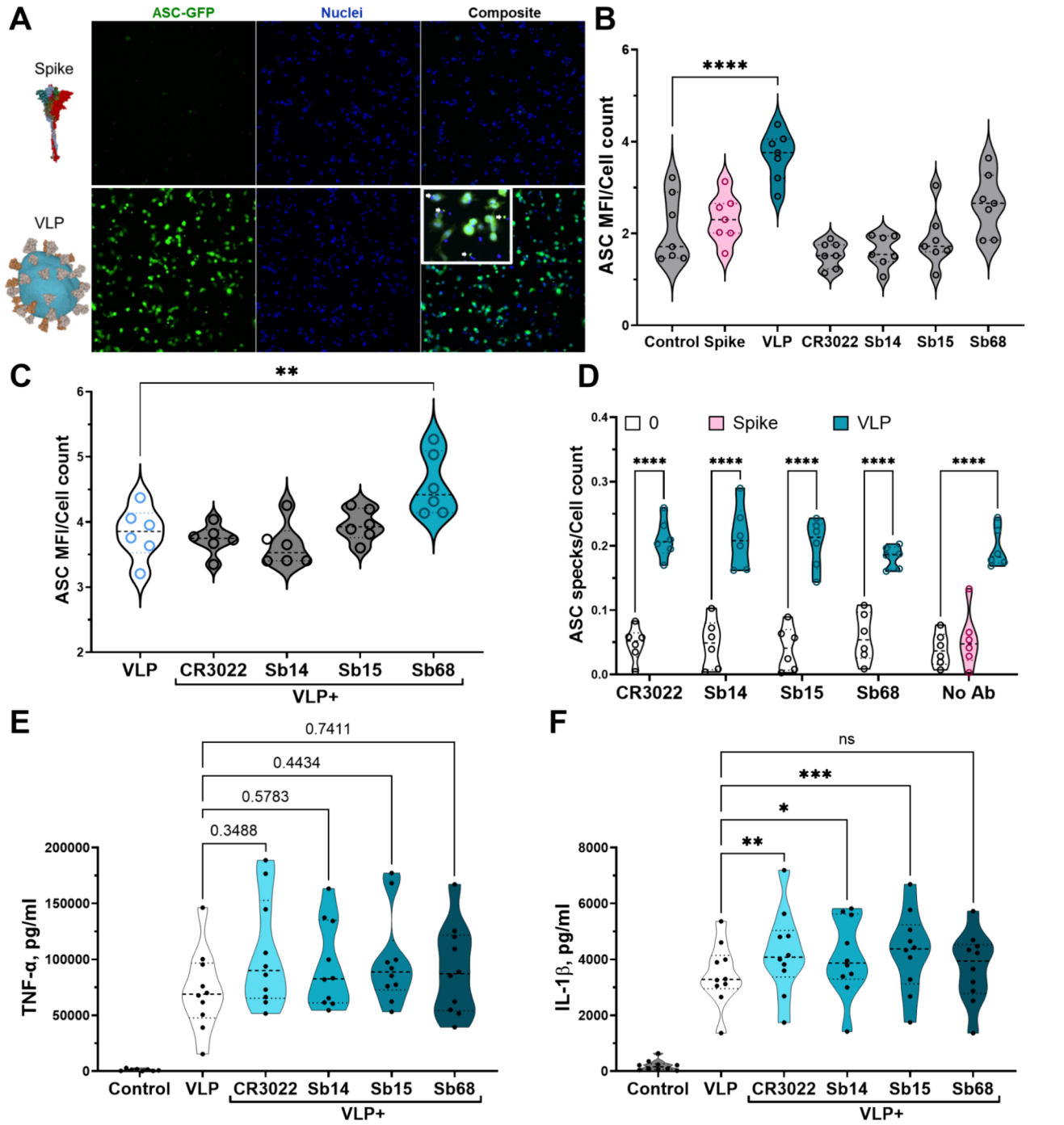

Figure 4. Inflammasome activation profile induced by VLPs and their ICs in THP-1 macrophages. THP-1-ASC-GFP macrophages were used for the evaluation of ASC protein fused with green fluorescent protein (ASC-GFP) expression and ASC speck formation. All cells were treated for 24 h with VLPs and their ICs or respective controls. (A) Representative image of ASC-GFP protein expression and ASC speck formation (white arrows) obtained using a wide-field microscope. Hoechst 33342 was used for nuclear staining to count the cells. (B, C) Quantification of ASC-GFP protein expression, mean fluorescent intensity (MFI) was calculated per cell number. (D) Quantification of ASC specks per cell number. (E,F) Secretion of inflammatory cytokines determined by ELISA: TNF-α (E) and IL-1β (F). Data are presented in violin plots with individual data points, $N = 6–10$ independent cell culture preparations. For panels (B, C, E, F), one-way ANOVA with Dunnett's multiple comparisons test was used. For panel (D), two-way ANOVA with Šídák's multiple comparisons test was used. $^{*}P < 0.05$, $^{**}P < 0.01$, $^{***}P < 0.001$, $^{****}P < 0.0001$. ns—not significant.

https://doi.org/10.1021/acsabm.6c00372
ACS Appl. Bio Mater. 2026, 9, 5196–5215

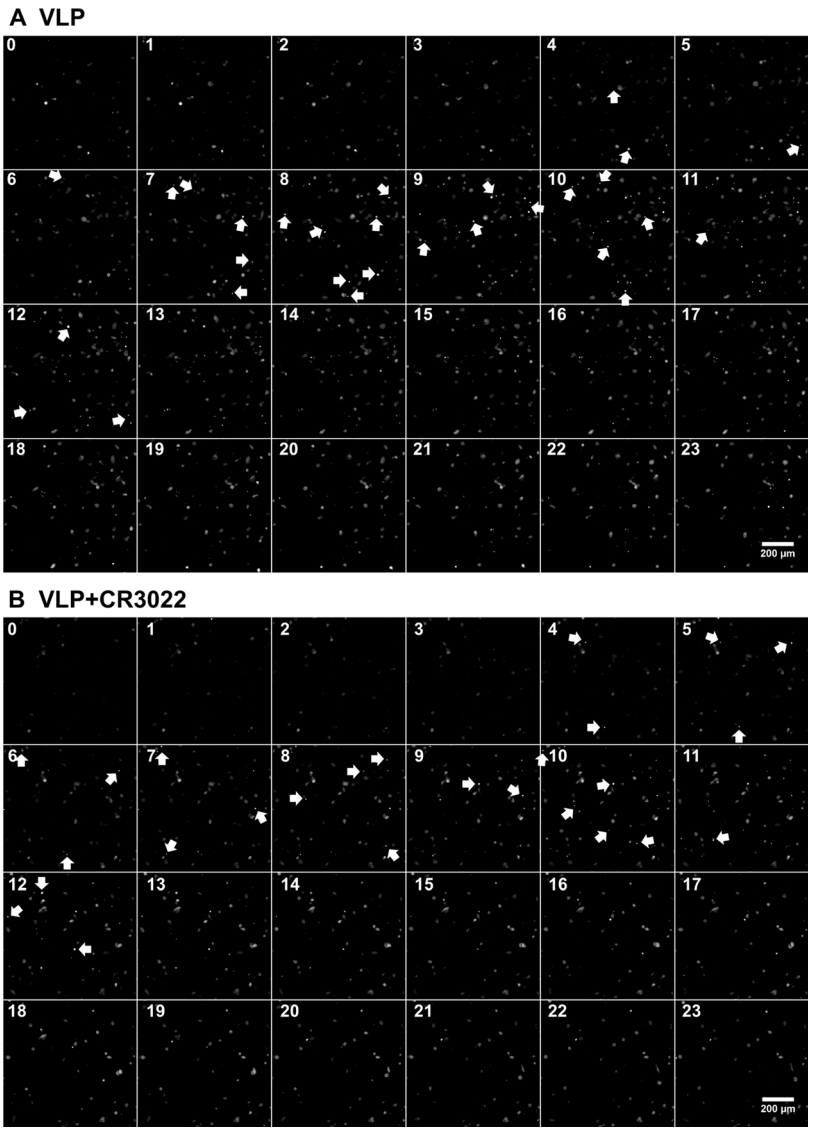

Figure 5. Time-lapse of inflammasome activation induced by VLPs and their ICs in THP-1-ASC-GFP macrophages. THP-1-ASC-GFP macrophages were used for the evaluation of the dynamics of ASC-GFP protein expression and ASC speck formation (white arrows). THP-1-ASC-GFP cells were imaged using a 20 × objective on a Nikon Eclipse Ti2-E wide-field fluorescence microscope. For each condition, six fields of view were captured and combined into a large image (2021 × 2021 μm, Supplementary Figure S1). The cropped images of 840 x 840 μm size are represented (Figure 5). The experiment included stimulation with VLPs (A) and an IC (B) formed using antibody CR3022. Images of live cells were taken hourly for 23 h. The number on the photos shows time points in hours.

by ICs, compared to VLPs, except in the case of IC formed by Sb68 (Figure 4). Interestingly, this IC also triggered higher expression of the ASC protein compared to other ICs (Figure 4). This demonstrates that VLPs induce an inflammasome activation profile that is affected by antibody opsonization, although opsonization does not inhibit inflammasome activation itself. Our results also show that both VLPs and ICs have the same effect on the secretion of the common inflammatory cytokine TNF-α.

To compare the immune response to VLPs and ICs over time, we performed a time-lapse experiment. THP-1-ASC-GFP macrophages were imaged hourly from 0 to 23 h post-exposure to monitor the dynamics of inflammasome activation. Images were acquired using a 20× objective on a Nikon Eclipse Ti2-E wide-field fluorescence microscope (Figure 5). For each condition, six fields of view were captured and combined into a single image (2021 × 2021 μm; Supplementary Figure S1). Representative cropped regions (840 × 840 μm) are shown in Figure 5. The experiment included stimulation with VLPs, and an IC formed using one of the antibody models CR3022. Inflammasome activation described by ASC speck formation was observed at 4 h post-exposure and became clearly pronounced from 6 h and reached its maximum at 12 h (Figure 5, white arrows). This timing is consistent with activation following phagocytosis, a relatively rapid cellular process. A similar kinetic profile has been reported for amyloid-β-induced inflammasome activation, which occurs within ∼6 h.[45] The protein expression of ASC-GFP was also visible within 6 h post VLPs and ICs exposure (Figure 5). Importantly, no significant differences in activation dynamics

https://doi.org/10.1021/acsabm.6c00372
ACS Appl. Bio Mater. 2026, 9, 5196−5215

were observed between VLP- and IC-treated cells across the analyzed time points.

Chemokine Secretion Profile Mediated by VLPs and ICs in Macrophages

To investigate chemokine secretion, we used the Chemokine Proteomic Profiler Array kit and simultaneously measured several chemokines in the collected cell culture supernatants. As a control, we used pure SARS-CoV-2 spike protein, as it did not induce an inflammatory signal in THP-1 macrophages (Figure 4B,D). We found that SARS-CoV-2 VLPs induce higher secretion of various chemokines compared to spike treatment (Figure 6B,D). However, antibodies that opsonized VLPs significantly reduced this effect, as ICs mediated a chemokine secretion profile similar to that of the control (Figure 6B,E). We also did not observe any differences between ICs formed by VLPs and those formed by Sb14 or Sb68. Therefore, only the IC of Sb14 was used for deeper characterization using bubble plots and volcano plots (Figure 6C,E). Additionally, some chemokines were not induced in THP-1 macrophages (the signal was equal to the negative control, known as the membrane background, Figure 6A). These chemokines were excluded from the analysis.

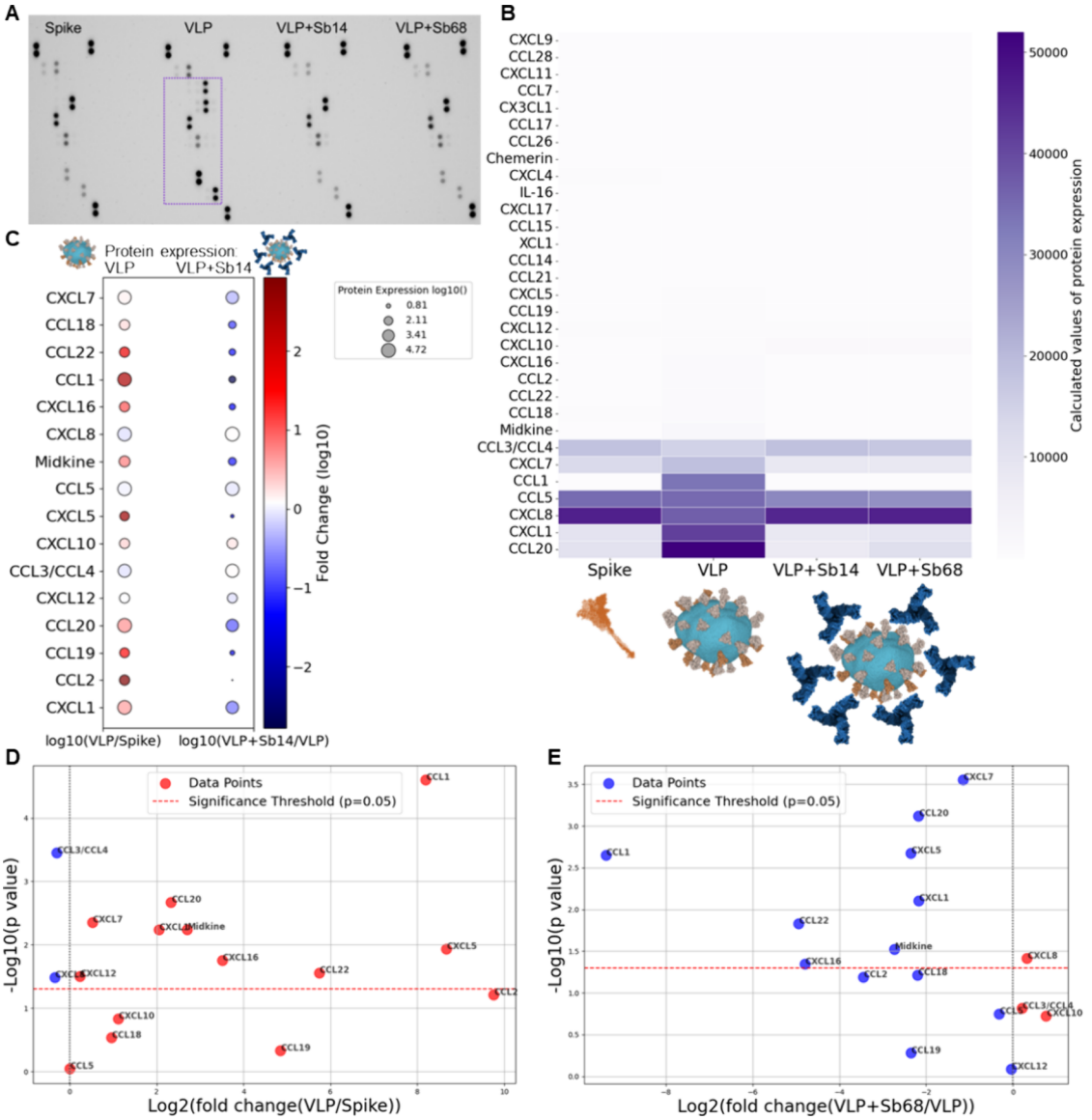

Figure 6. Chemokine secretion proteomic profile mediated by VLPs and their ICs in THP-1 macrophages. Cells were treated for 24 h with VLPs and their ICs or the respective control (spike protein). The Chemokine proteome profiler array was used to measure chemokine secretion in a mixture of supernatants of 5 independent cell culture preparations per treatment condition. (A) Representative raw blot of the assay. Most of the chemokines induced by VLPs are in the violet rectangle. Each chemokine was measured twice (two spots). (B) Heatmap of quantified chemokine expression values from raw blots. Negative values (background spots noted by the manufacturer) of each membrane were extracted from quantified values. (C) Bubble plots showing both protein expression and fold changes in log10 values. In the fold change log10(VLP/Spike), the bubble size shows protein expression after cell treatment with VLP, the color—fold change of log10(VLP/Spike); in the fold change log10(VLP + Sb14/VLP), the bubble size shows protein expression after cell treatment with IC formed by VLP and Sb14, and the color—fold change of log10(VLP + Sb14/VLP). (D, E) Volcano plots showing fold changes and calculated p values according to the *t*-test. Blue color represents a decrease (negative values), and red color represents an increase in protein expression (positive values).

https://doi.org/10.1021/acsabm.6c00372
ACS Appl. Bio Mater. 2026, 9, 5196−5215

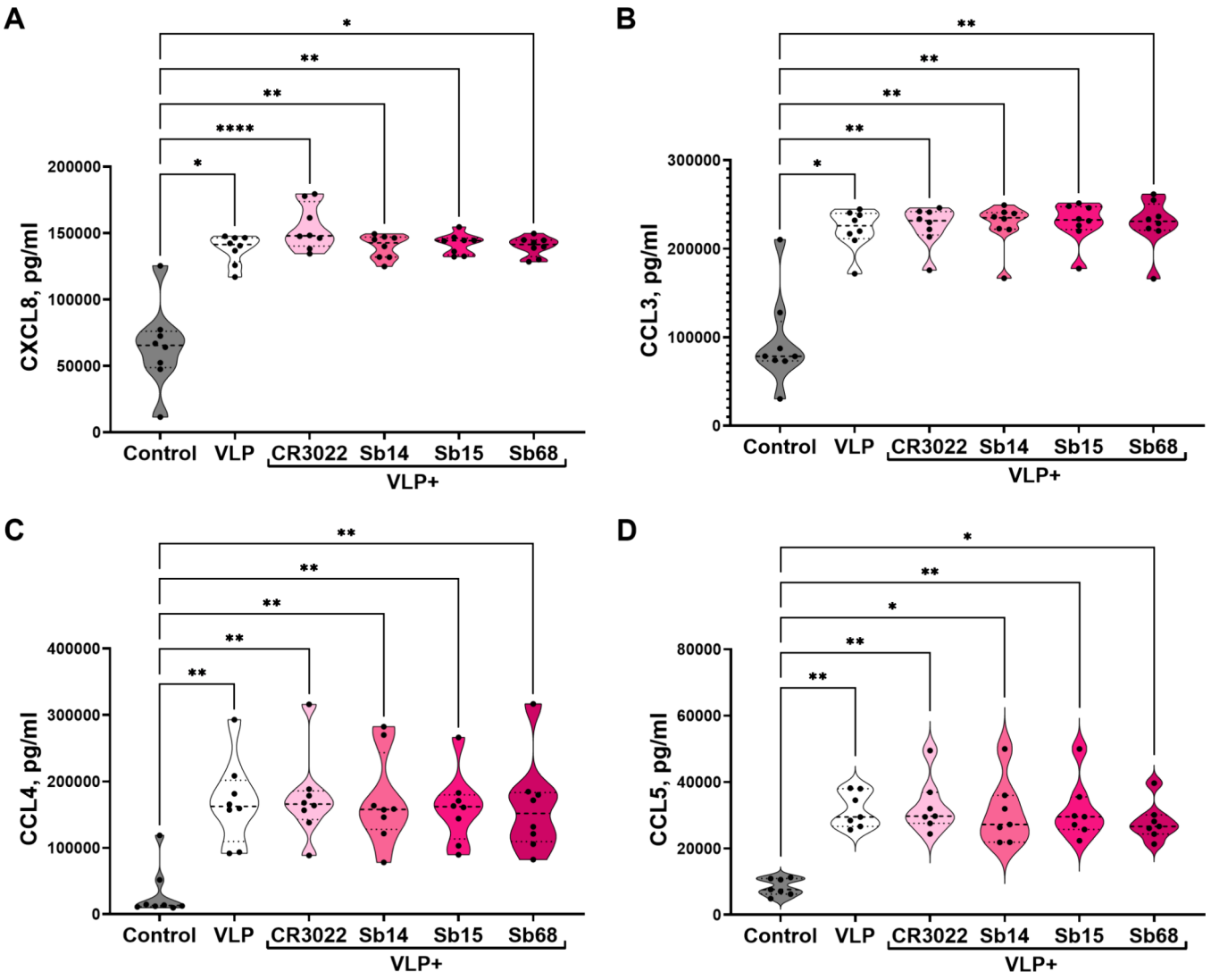

Figure 7. Chemokine secretion was determined by ELISA in THP-1 macrophages. Cells were treated for 24 h with VLPs and their ICs or control (untreated cells). Chemokine secretion was determined in collected cell culture supernatants: (A) CXCL8, (B) CCL3, (C) CCL4, and (D) CCL5. Data are presented in violin plots with individual data points, $N = 7$ independent cell culture preparations. A non-parametric Kruskal–Wallis test with Dunn's post-hoc test was used, $^{*}P < 0.05$, $^{**}P < 0.01$, $^{***}P < 0.001$, $^{****}P < 0.0001$.

VLPs also had no effect on the secretion of some chemokines, or a lower amount was detected compared to control treatment (Spike, Figure 6C). Among them were CXCL8, CCL3/CCL4, and CCL5. On the other hand, the spots of these chemokines were very bright, indicating that a very high level of protein was detected in the supernatants of all treatments. In this case, the detection-level error can occur, while a diluted sample may provide more accurate results. Additionally, ICs had a similar effect on the release of CXCL8, CCL3/CCL4, and CCL5 chemokines compared to VLPs. Additionally, ICs induced a slightly higher secretion of CXCL10 (Figure 6). To confirm these results, we measured the concentrations of CXCL8, CCL3, CCL4, CCL5, and CXCL10 in supernatants by ELISA.

ELISA data revealed that VLPs mediated a higher release of CCL3, CCL4, CCL5, and CXCL8 compared to control cells (Figure 7). Additionally, control cells also secreted high levels of these chemokines, confirming the results of the proteomic profiler assay (Figure 6C). Both VLPs and ICs had the same effect on the secretion of these chemokines. Additionally, IC formed by CR3022 induced a higher release of CXCL8, but the result was not significant (Figure 7). CXCL10 secretion was below the detection limit of the used assay. Overall, our data on chemokine secretion profile shows that VLP opsonization by antibodies affects the release of some of the VLP-induced chemokines.

Expression of Cellular Markers Related to Antigen Presentation and Chemokine Receptors Induced by VLPs and Their ICs in Macrophages

To evaluate antigen presentation, we measured the cell surface expression of co-stimulatory molecules CD86 and CD83. CD86 expression also indicates an inflammatory response, whereas CD83 is a regulatory molecule involved in antigen presentation, and its presence is associated with a resolution of inflammation after infection. The expression of these markers was measured at a single-cell level using flow cytometry.

https://doi.org/10.1021/acsabm.6c00372
ACS Appl. Bio Mater. 2026, 9, 5196−5215

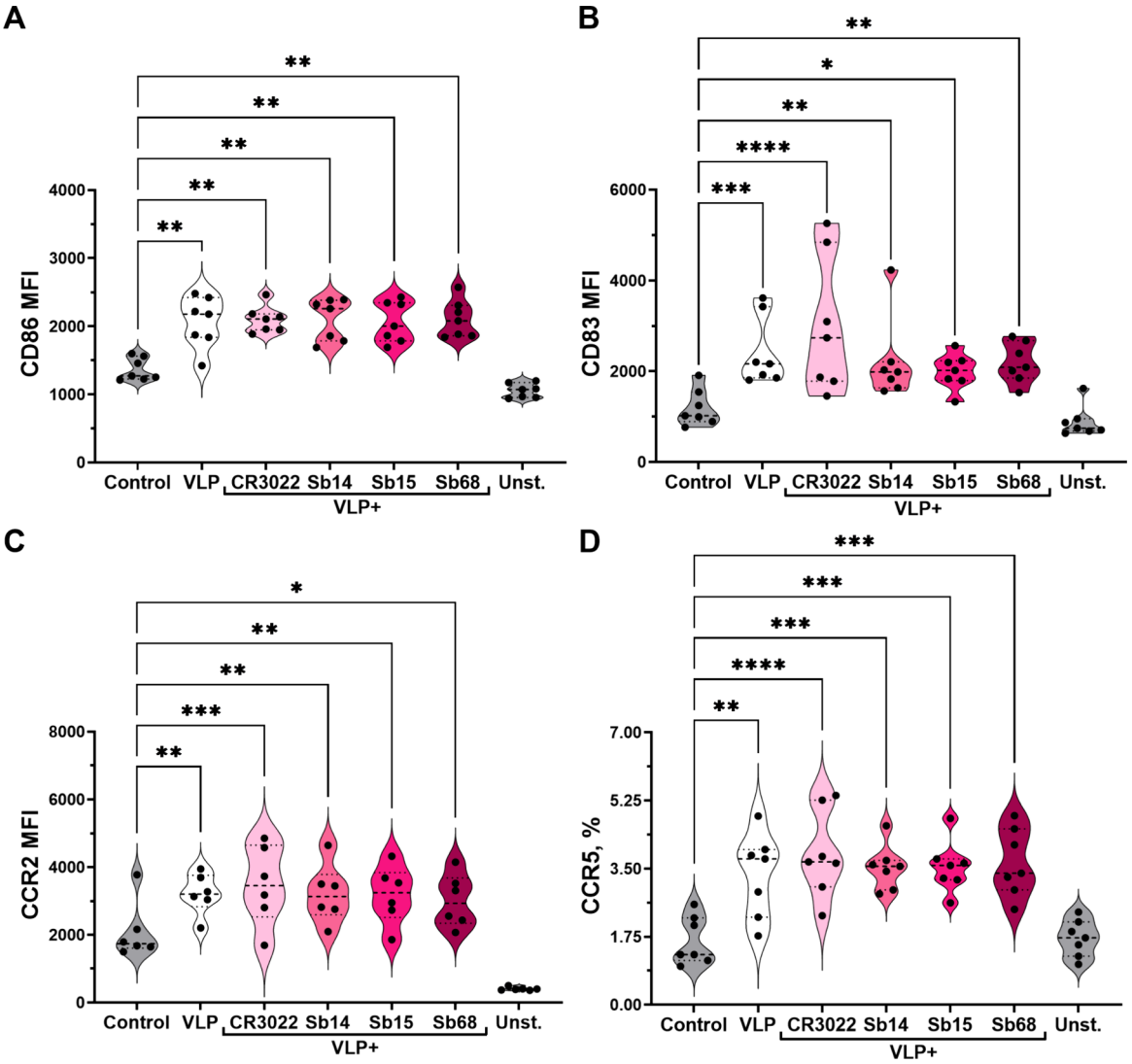

Figure 8. Cell surface expression of antigen presentation-related molecules and chemokine receptors induced by VLPs and their ICs in THP-1 macrophages. Cells were treated for 24 h with VLPs and their ICs or control (untreated cells). The cells were collected for flow cytometry analysis of marker expression on the cell surface. Quantified data are shown: (A) CD86 (MFI—mean fluorescent intensity), (B) CD83 (MFI), (C) CCR2 (MFI), and (D) CCR5 (fraction of positive cells, %). Unst.—unstained cells that were incubated with respective antibody isotype controls. Data are presented in violin plots with individual data points, $N = 6–7$ independent cell culture preparations. One-way ANOVA with Dunnett's multiple comparisons test was used, $^{*}P < 0.05$, $^{**}P < 0.01$, $^{***}P < 0.001$, $^{****}P < 0.0001$.

We found that VLPs significantly increased both CD86 (Figure 8A) and CD83 (Figure 8B) expression compared to the control, while ICs had the same effect as VLPs.

We also measured the expression of chemokine receptors on the cell surface at the single-cell level. We selected CCR2, as VLPs mediated CCL2 secretion in our cell model (Figure 6C). As it was shown in previous research, the CCR2 expression may be related to CD83 expression.[46,47] CCR5 was selected for investigation of the CCL5/CCR5 axis, as we observed a significant increase in secretion of CCL5 following macrophage treatment with VLPs and ICs. We detected that VLPs and ICs significantly increased expression of both CCR2 (Figure 8C) and CCR5 (Figure 8D); however, only a small fraction of CCR5-positive cells was found. Comparing different ICs, we haven't observed the differences in their induced expression of the analyzed markers.

Next, we performed a multiple variable analysis to characterize the distribution of the expression of cell surface markers among different treatments. We found that, depending on the treatment, there is an association between CCR2 and CD83 as the dots cluster together in the CCR2 vs CD83 plot (Figure 9A). Pearson correlation analysis demonstrated a positive correlation between the expression of these markers (correlation coefficient $R = 0.7$). We also performed a multiple variable analysis for other markers and found some relationships. Addition of IL-1β and TNF-α concentration values showed that cells, having, on average, low CCR2 and CD83 expression, secreted less IL-1β but more TNF-α (blue ellipse, Figure 9B). Also, this was the case with CCL5 secretion, as these cells secreted a lower amount of CCL5 than the others (blue ellipse, Figure 9C). Plotting IL-1β vs TNF-α showed that the markers clustered into two distinct groups (blue ellipses,

https://doi.org/10.1021/acsabm.6c00372
ACS Appl. Bio Mater. 2026, 9, 5196−5215

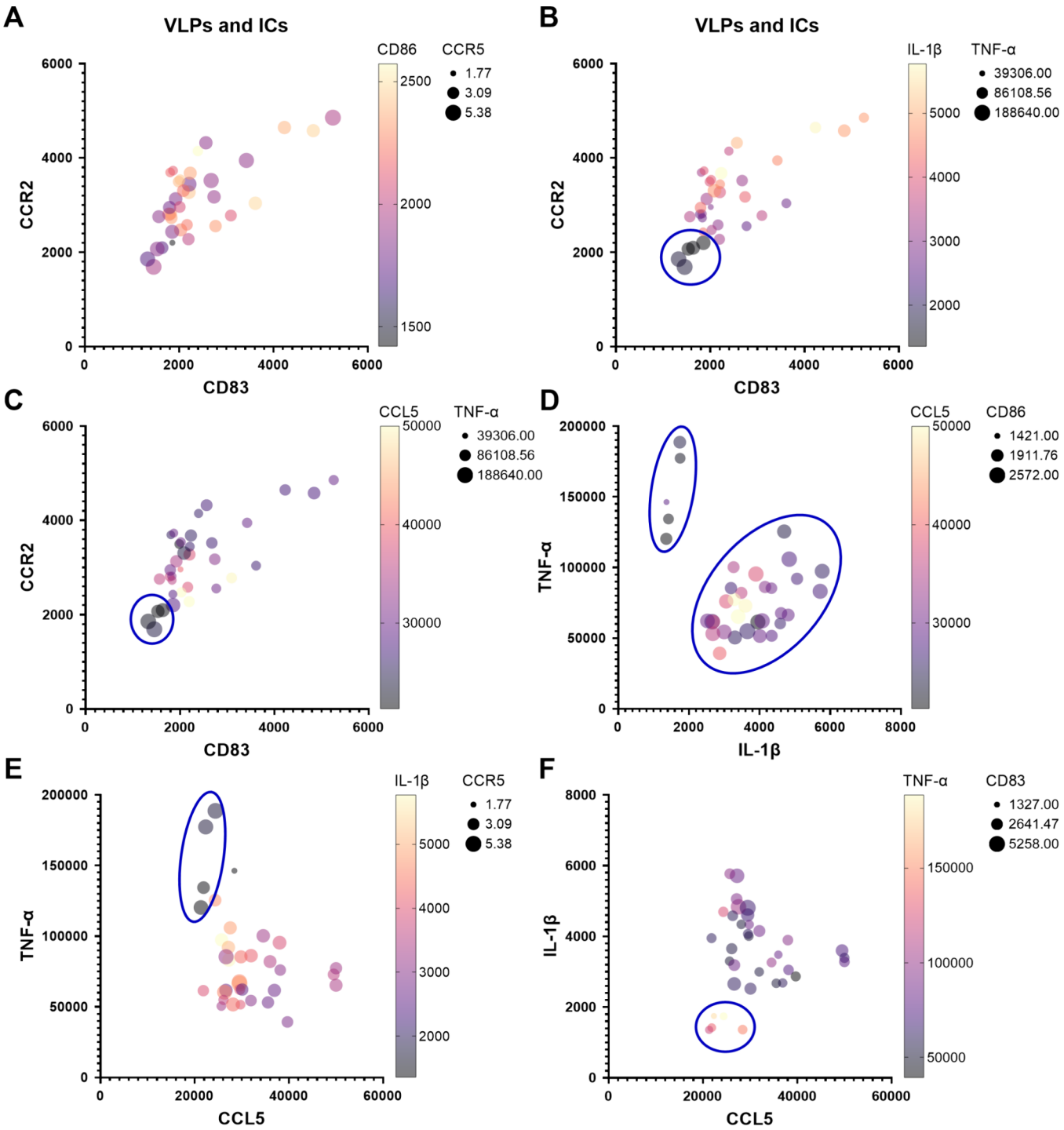

Figure 9. Multiple variable analysis of macrophage activation markers. Values of marker expression after THP-1 macrophage treatment with VLPs or different ICs (of VLPs and one of the antibody models: CR022, Sb14, Sb15, or Sb68) were put into one graph. Markers: cell surface expression of CCR2 (MFI—mean fluorescent intensity), CD83 (MFI), CD86 (MFI), CCR5 (fraction of positive cells, %), and secretion of IL-1β, TNF-α, and CCL5 (in pg/ml). Plots of a combination of different markers are shown in panels (A–F). Dot colors and sizes represent marker intensity, as shown in the legends. Blue ellipses indicate the formed clusters based on the expression level of the markers.

Figure 9D). One of the clusters showed cells that secreted a low amount of IL-1β, but high levels of TNF-α and a relatively low amount of CCL5 (Figure 9D). The other cells secreted moderate to high levels of IL-1β and TNF-α, while the cells secreting very high levels of IL-1β also expressed a higher amount of CD86. Plotting CCL5 vs TNF-α and adding CCR5 expression revealed a variable distribution of marker expression, with very high expression of CCR5 in cells secreting high levels of TNF-α and low levels of CCL5 (blue ellipse, Figure 9E). Plotting CCL5 vs IL-1β and adding CD83 expression showed that the cells, which secreted, on average, very low levels of IL-1β and high levels of TNF-α, had low expression of CD83

https://doi.org/10.1021/acsabm.6c00372
ACS Appl. Bio Mater. 2026, 9, 5196−5215

(blue ellipse, Figure 9F). They also secreted lower levels of CCL5, although other cells that secreted lower levels of CCL5 also secreted very high levels of IL-1β. These data show that cells with higher average CD83 expression also secrete higher levels of TNF-α, but lower levels of IL-1β and CCL5. This relationship is observed only with the regulatory molecule of the inflammatory response, CD83, but not with CD86, which is associated with the inflammatory macrophage phenotype.

DISCUSSION

Antibodies can engage FcRs to trigger antiviral effector functions, a phenomenon observed across various viruses known for many years. These antibody-mediated effector functions, mediated via the Fc fragment interaction with FcR, are essential for protection against viral infections. However, the detailed mechanisms by which Fc-mediated processes operate in innate immune cells remain incompletely understood. This knowledge gap limits the potential of using antibodies as universal tools for antiviral therapy and raises concerns about the safety of vaccines that rely on antibody-mediated protection. Here, we studied several immunological processes and their relationships, including the antibody–antigen interaction and the effect of IC multivalence, the IC interaction with FcRs, and the antibody-mediated effector function in macrophages, which leads to the generation of inflammatory signals.

Coronaviruses, including SARS-CoV-2, infection-induced hyperinflammation is associated with the production of a plethora of chemokines that recruit various immune cells to the site of infection via interaction with cellular chemokine receptors.[48] Furthermore, the inflammatory response, together with the chemotactic response to SARS-CoV-2, has been demonstrated in many in vivo and in vitro models.[49] The role of chemokines in inflammatory conditions has been emphasized by the chemokine interactome map. Inflammation has been shown to be related to the recruitment of immune cells through the chemokine axis, and chemokines interact with each other, leading to the activation or inhibition of cellular receptors involved in inflammatory processes.[50] Our data show that SARS-CoV-2 VLPs, which represent a virus structure recognized by cellular receptors, induce the secretion of a variety of chemokines, whereas antibody-opsonized VLPs have a contrary effect. Some chemokines can trigger other inflammatory processes, for example, CXCL1 and CXCL2 can drive inflammasome activation in macrophages.[51] Studies also show that very high levels of inflammatory chemokines are detected in the serum of patients with severe COVID-19.[52] Moreover, the role of innate immunity in causing inflammatory conditions was demonstrated in various coronavirus infections during which innate immune cells secrete inflammatory cytokines, together with inflammasome activation[53] associated with COVID-19 severity.[54] Our results also showed inflammasome activation induced by SARS-CoV-2 VLPs; however, antibody-opsonized VLPs had the same impact as VLPs alone, contrary to the chemokine reduction effect. Inflammasome activation leads to inflammatory cell death, known as pyroptosis, which has been demonstrated to be one of the drivers of the cytokine storm observed in SARS-CoV-2 infection.[55] Our results on inflammasome activation mediated by both VLPs and their ICs confirm that antibodies may enhance inflammasome activation detected in COVID-19. As antibodies did not reduce inflammasome activation, which is one of the triggers of hyperinflammation,[56] the alternative therapies for severe COVID-19 disease should be considered. Additionally, knowledge of the precise mechanisms of antibody-mediated effector functions would be useful in creating engineered antibodies, as they have been shown to be promising tools for preventing or treating viral infections.[57]

Chemokines secreted by macrophages can recruit other immune cells and induce paracrine or autocrine signals by binding to chemokine receptors on the cell surface. As we found chemokine production induced by VLPs, we also investigated the expression of cellular chemokine receptors. It has been shown that CCR2 and CCR5 can be expressed on macrophages and are elevated during their activation.[58] They also participate in the macrophage polarization process. Increased expression of CCR2 and CCR5, as well as secretion of CXCL8 and CCL2, shows a pro-inflammatory state of macrophages. These molecules were induced by our VLPs and their ICs, confirming the inflammatory phenotype of macrophages. During COVID-19, high expression of these markers was also observed on immune cells, as well as a plethora of other chemokine receptors and secreted chemokines themselves.[59] In other viral infections, the expression of observed chemokines and their receptors is generally limited in variety, compared to SARS-CoV-2 infection. CCR5 was found to be expressed on immune cells during HIV infection, while CCR2 was expressed during other coronavirus infections. This demonstrates the exclusivity of SARS-CoV-2 and the prominence of its investigation. The comprehensive analysis of lung-resident macrophages, which, together with recruited monocytes, play a crucial role during COVID-19 disease, revealed the existence of distinct macrophage populations characterized by different expression patterns of chemokines and their receptors.[60] The coordinated production of chemokines was also found to regulate the influx of immune cells into the lungs during inflammatory conditions. Looking at the innate immune signatures of severe COVID-19 patients, there were no differences in expression of chemokine receptors in dendritic cells; however, it was different among monocyte populations.[61] Pro-inflammatory CCR2 was found to be reduced in severe cases of COVID-19. Overall, CCL2 levels are elevated in the serum, and CCR2 expression is observed in the blood cells of patients infected with SARS-CoV-2.[62] Moreover, increased expression of CCR2 is related to monocyte/macrophage recruitment to the lungs in COVID-19.[63] Consequently, the CCL2/CCR2 axis represents a promising target for intervention. While both CCL2 and CCR2 are highly expressed by macrophages, in the context of the CCL5/CCR5 axis, it is primarily CCL5 that is secreted by macrophages under inflammatory conditions. On the other hand, CCR5 is predominantly expressed on T cells and plays a critical role in T cell recruitment to the infection site, as demonstrated in the context of COVID-19.[63] Also, in COVID-19, it was assumed that recruited CCR5-positive T cells stimulate antibody production by plasma cells, while antibodies contribute to activation of macrophages, leading to strong inflammation and enhancement of other inflammatory diseases.[64] Our findings demonstrate that macrophages express CCR5 and highly secrete CCL5 upon stimulation with SARS-CoV-2 VLPs. This response appears to be intrinsic to macrophage activation, as VLP opsonization by antibodies did not significantly modify CCR5 expression or CCL5 secretion. Our observations suggest that SARS-CoV-2 components can directly trigger the CCR5/CCL5 signaling axis in macrophages, independent of antibody involvement, which

https://doi.org/10.1021/acsabm.6c00372
ACS Appl. Bio Mater. 2026, 9, 5196−5215

may contribute to the pro-inflammatory conditions observed during infection.

SARS-CoV-2 enters cells through interaction of the spike protein with the ACE2 receptor on the cell surface. After that, the SARS-CoV-2 virus enters endosomes, and the cell signaling cascade is activated. One of them is NF-κB pathway activation, followed by the expression of inflammasome components, including the NLRP3 protein and IL-1β.[65] This pathway was detected by VLPs in our study, emphasizing the suitability of VLPs to investigate the molecular mechanisms of innate immune cell activation by the SARS-CoV-2. In addition, a comprehensive analysis of serum cytokines during the COVID-19 disease course revealed elevated levels of inflammatory molecules, including CXCL8, TNF-α, and IL-6.[66,67] Additionally, macrophage-secreted IL-1β upon inflammasome activation may activate adjacent cells to produce inflammatory cytokines, including CXCL8, TNF-α, and IL-6,[68] which are important for the recruitment of other innate immune cells, like neutrophils. We also found that CXCL8 and TNF-α production is mediated by SARS-CoV-2 VLPs, which makes VLPs comparable to virion-induced innate immune cell activation. There are numerous potential research areas that can be translated into the development of medicines, which modulate immune cell activation. For example, it is essential to understand the role of the inflammasome in humoral immunity, as its signals can stimulate the adaptive immune system.[69] Our results indicate that noninfectious VLPs may be a potential tool for investigating cross talk between the innate and adaptive immune systems.

Macrophages are also antigen-presenting cells.[2] After antigen phagocytosis and processing in endosomes, it can be exposed on the cell surface to T cells.[3] For efficient T cell activation, co-stimulatory molecules are required. Additionally, regulatory molecules participate in this process to prevent excessive cell activation and uncontrolled inflammatory reactions. In our study, we investigated the expression of co-stimulatory molecules CD86 and CD83 on the cell surface after activation with VLPs and their ICs. We found that both VLPs and ICs induced exposure of CD86 and CD83 on the cell surface at the same level. CD86 is also related to the inflammatory response in macrophages; however, the function of CD83 is the opposite. It is a regulatory molecule that plays an important role in the resolution of inflammation.[70] CD83 was shown to be an important immune checkpoint in COVID-19,[71] while co-stimulation of CD86 together with CD80 contributes to hyperinflammation observed in severe SARS-CoV-2 infection, while blocking these molecules is a promising therapeutic strategy.[72] It was also shown that in macrophages, CD83 is expressed during the early stages of cell activation and influences the subsequent cellular response.[73] Its deletion impairs macrophage plasticity and has a negative impact on the resolving properties after induced inflammation.[42] This can lead to chronic inflammatory conditions. For example, it has been demonstrated that CD83-deficient brain-resident macrophages, specifically microglia, contribute to neuroinflammation by recruiting overactivated immune cells.[46] Interestingly, in our study, SARS-CoV-2 VLPs induced both cellular molecules, CD86 and CD83, participating in inflammatory conditions and their resolution. It is possible that, under certain circumstances, this balance is altered, leading to hyperinflammation, tissue damage, and ultimately cell apoptosis and fibrosis.

Large conformational changes are described during antibody binding to the antigen, but each case is unique.[74] Conformational changes can occur in the antibody binding region, the Fc region or in both.[75] The conformational changes in the Fc region can also influence the binding of the antibody Fc fragment to FcR and subsequent antibody-mediated effector function in target cells. This can affect the affinity of the antibody Fc region to FcR, which is one of the driving factors influencing the activation of immune effector cells engaged by ICs.[76] Another noteworthy fact is that antibodies with different constant domains also exhibit different affinities.[77,78] All these factors highlight the importance of knowing conformational changes during antibody–antigen interaction for deeper characterization of antibody activity. Here, we employed the QCM-D parameter ΔD to compare antibody affinity, along with viscoelasticity associated with conformational changes of the interacting molecules. Even though the Fc part of all VHH-Fc antibody models, used in our study, was identical and they targeted the same specific antigen, there were significant differences in the amount of VLP bound to the antibodies and also in ΔD. This is likely due to differences in their paratope structures, which can influence how each antibody interacts with the antigen at the molecular level, including the precise shape and binding interface of the antigen–antibody complex.[75] During IC formation, the sudden increase in rigidity, as we showed by $\Delta D/\Delta F$ plots of VLP–antibody interaction, can be explained by the VLP antigens reaching a percolation threshold, at which point a connected network of bound complexes spans the surface, leading to an abrupt change in viscoelasticity.[79] The VHH-Fc antibody model Sb68, which distinguished itself from the others in terms of dissipation, also had a different effect on the inflammatory response in macrophages, providing insights into IC properties and their relationship to cell activation.

FcR involvement was not directly tested in this study. However, several aspects of our data suggest that FcR-mediated signaling may contribute to the observed effects. FcγR engagement is required for IC-induced activation in similar cellular contexts, supporting the likelihood that Fc-dependent pathways play a role. In particular, the differences observed among the investigated ICs across antibodies with respect to cell activation indicate that the response is antibody specific. This is consistent with mechanisms influenced by Fc-dependent properties such as FcγR binding affinity and avidity. Engagement of FcγR by ICs is known to trigger downstream signaling cascades that modulate cellular activation and effector functions, further supporting the plausibility of this pathway in our system. At the same time, we cannot exclude contributions from Fc-independent mechanisms, including activation driven by free antigen, which may act in parallel with or independently of FcR signaling. Moreover, antibody–antigen interactions are reversible, making it difficult to precisely define the relative contributions of ICs vs free antibody and antigen during their interaction with cellular receptors. Overall, our findings are consistent with a role for FcR engagement; however, definitive attribution of the observed effects to Fc-dependent mechanisms remains to be established.

The data presented here indicate that SARS-CoV-2 VLPs activate macrophages through multiple innate immune signaling pathways initiated upon particle recognition and uptake. As multivalent nanostructures resembling native virions, VLPs engage pattern recognition receptors (PRRs), leading to activation of downstream signaling cascades, including NF-κB-dependent transcription of pro-inflammatory mediators and priming of inflammasome components. Consistent with this mechanism, VLP exposure increased ASC expression and TNF-

https://doi.org/10.1021/acsabm.6c00372
ACS Appl. Bio Mater. 2026, 9, 5196−5215

α secretion, followed by IL-1β release and ASC speck formation, demonstrating canonical inflammasome activation. Antibody opsonization of VLPs did not suppress inflammasome signaling, indicating that FcγR engagement provides an additional activating signal. In our system, ICs preserved TNF-α secretion and enhanced IL-1β production relative to VLPs alone, with the magnitude of inflammasome activation dependent on the structural properties of the formed ICs. These findings support a model in which PRR-derived priming signals and FcγR-mediated activation converge at the level of inflammasome assembly. Notably, antibody-opsonized VLPs markedly reduced inflammatory chemokine secretion, suggesting an uncoupling of inflammasome activation from sustained transcriptional chemokine responses. This divergence highlights how IC architecture modulates macrophage signaling outputs. In parallel, both VLPs and ICs induced surface expression of CD86 and CD83. CD86 contributes to costimulatory signaling and inflammatory activation, whereas CD83 functions as a regulatory molecule involved in controlling immune responses and promoting resolution. The coexpression of both markers suggests that SARS-CoV-2 VLPs drive a coordinated macrophage activation state encompassing inflammation, inflammasome signaling, and antigen-presenting cell maturation. As monomeric spike protein and its ICs failed to elicit comparable activation, these results underscore the importance of antigen multivalency, IC structure, and Fc-mediated interactions in shaping macrophage responses—key considerations for immunologically active biomaterials, nanovaccines, and antibody-based therapeutics.

CONCLUSIONS

We investigated the inflammatory mechanisms induced by SARS-CoV-2 VLPs and their ICs, which are relevant to the innate immune response to viral infections and the associated strong inflammation. The focus was on the inflammatory response, including inflammasome activation, antigen presentation, and the role of chemokines in the macrophage activation pathway. We found that VLPs induced strong expression of inflammatory molecules and activated the inflammasome, as did their ICs. Also, that antibodies can enhance SARS-CoV-2 VLP-mediated IL-1β release, which is consistent with our previous research, where we used human polyomavirus VLPs as an antigen model. We likewise found that ICs had a reverse effect on inflammatory chemokine secretion compared to SARS-CoV-2 VLPs, contrary to inflammasome activation, which seems to be irrelevant to chemokine signals. Interestingly, SARS-CoV-2 VLPs and their ICs induced cell surface expression of both costimulatory molecules related to antigen presentation, CD86 and CD83. CD86 also exhibits an inflammatory response, which aligns with other effects induced by VLPs Figure 9. In contrast, CD83 expression is associated with a resolution of inflammation and has a positive impact on preventing the development of severe inflammation. We showed that this effect induced by SARS-CoV-2 antigen and formed multivalent ICs for the first time. We anticipate that our findings on factors influencing antibody-mediated immune cell effector functions will broaden the horizons in the field of innate immunity research and provide new insights for both fundamental and clinical studies, clarifying the immunopathology caused by viral infections and evaluating the adverse reactions of vaccines.

ASSOCIATED CONTENT

Data Availability Statement

All data used to support the findings of this study are included within the article and Supporting Information.

Supporting Information

The Supporting Information is available free of charge at https://pubs.acs.org/doi/10.1021/acsabm.6c00372.

Wide-field fluorescence microscope images; figure arts used from these resources: BIOART-000308: NIAID Visual & Medical Arts. (10/7/2024). Macrophage. NIAID NIH BIOART Source. bioart.niaid.nih.gov/bioart/308; BIOART-00007: NIAID Visual & Medical Arts. (10/7/2024). Cell Death. NIAID NIH BIOART Source. bioart.niaid.nih.gov/bioart/71; BIOART-000123: NIAID Visual & Medical Arts. (10/7/2024). DNA. NIAID NIH BIOART Source. bioart.niaid.nih.gov/bioart/123; BioVisUser123. Human Heart Model [3D model]. Version 2.01. NIH 3D. Published 2021. Accessed October 13, 2025. 3DPX-016453 https://3d.nih.gov/entries/16453; BioVisUser123. Human Heart Model [3D model]. Version 2.01. NIH 3D. Published 2023. Accessed October 13, 2025. 3DPX-013323 https://3d.nih.gov/entries/13323; BioVisUser 123. Human Heart Model [3D model]. Version 2. NIH 3D. Published 2023. Accessed October 13, 2025. https://3d.nih.gov/entries/3DPX-012086 3DPX-012086; and BioVisUser123. Human Heart Model [3D model]. Version 2. NIH 3D. Published 2023. Accessed October 13, 2025. 3DPX-017681 https://3d.nih.gov/entries/3DPX-017681 (DOCX)

AUTHOR INFORMATION

Corresponding Authors

Asta Lučiūnaitė – *State Research Institute Center for Physical Sciences and Technology, Sauletekio Ave. 3, Vilnius 10257, Lithuania; Institute of Biotechnology, Life Sciences Center, Vilnius University, Sauletekio Ave. 7, Vilnius 10257, Lithuania;* Email: asta.luciunaite@bti.vu.lt

Ieva Plikusiene – *State Research Institute Center for Physical Sciences and Technology, Sauletekio Ave. 3, Vilnius 10257, Lithuania; Faculty of Medicine, Pharmacy and Pharmacology Center, Vilnius University, M. K. Ciurlionio str. 21, Vilnius 03101, Lithuania;* orcid.org/0000-0002-7972-8891; Email: ieva.plikusiene@chgf.vu.lt

Authors

Mantvydas Usvaltas – *State Research Institute Center for Physical Sciences and Technology, Sauletekio Ave. 3, Vilnius 10257, Lithuania*

Vincentas Maciulis – *State Research Institute Center for Physical Sciences and Technology, Sauletekio Ave. 3, Vilnius 10257, Lithuania;* orcid.org/0000-0001-9552-8649

Complete contact information is available at: https://pubs.acs.org/doi/10.1021/acsabm.6c00372

Author Contributions

A.L.: Conceptualization; data curation; investigation; methodology; writing-original draft; writing—review and editing; and funding acquisition. M.U.: Investigation; methodology;writing-

original draft; writing—review and editing; and visualization. V.M.: writing-original draft; Writing—review and editing; visualization; and methodology. I.P.: Supervision; methodology; writing-original draft; writing—review and editing; and funding acquisition.

Funding

This work was funded by the Research Council of Lithuania, postdoctoral fellowship project No. S-PD-24-156.

Notes

This study does not involve animal/human research.
The authors declare no competing financial interest.

■ ABBREVIATIONS

FcR	Fc receptor
IC	immune complex
PRRs	pattern recognition receptor
SE	spectroscopic ellipsometry
VLP	virus-like-particle
VHH-Fc	nanobody (VHH) Fc fusion protein
QCM-D	quartz crystal microbalance with dissipation

■ REFERENCES

(1) Tay, M. Z.; Wiehe, K.; Pollara, J. Antibody-Dependent Cellular Phagocytosis in Antiviral Immune Responses. *Front. Immunol.* **2019**, *10*, No. 332.
(2) Lendeckel, U.; Venz, S.; Wolke, C. Macrophages: shapes and functions. *ChemTexts* **2022**, *8* (2), 12.
(3) Junker, F.; Gordon, J.; Qureshi, O. Fc Gamma Receptors and Their Role in Antigen Uptake, Presentation, and T Cell Activation. *Front. Immunol.* **2020**, *11*, No. 1393.
(4) Ragab, D.; Salah Eldin, H.; Taeimah, M.; Khattab, R.; Salem, R. The COVID-19 Cytokine Storm; What We Know So Far. *Front. Immunol.* **2020**, *11*, No. 1446.
(5) Hussman, J. P. Severe Clinical Worsening in COVID-19 and Potential Mechanisms of Immune-Enhanced Disease. *Front Med (Lausanne)*. **2021**, *8*, No. 637642.
(6) Junqueira, C.; Crespo, Â.; Ranjbar, S.; de Lacerda, L. B.; Lewandrowski, M.; Ingber, J.; Parry, B.; Ravid, S.; Clark, S.; Schrimpf, M. R.; et al. FcγR-mediated SARS-CoV-2 infection of monocytes activates inflammation. *Nature* **2022**, *606* (7914), 576–584.
(7) Ferreira, A. C.; Soares, V. C.; de Azevedo-Quintanilha, I. G.; Dias, S. D. S. G.; Fintelman-Rodrigues, N.; Sacramento, C. Q.; Mattos, M.; de Freitas, C. S.; Temerozo, J R; Teixeira, L.; et al. SARS-CoV-2 engages inflammasome and pyroptosis in human primary monocytes. *Cell Death Discov.* **2021**, *7* (1), No. 43.
(8) Sefik, E.; Qu, R.; Junqueira, C.; Kaffe, E.; Mirza, H.; Zhao, J.; Brewer, J R; Han, A.; Steach, H. R.; Israelow, B.; et al. Inflammasome activation in infected macrophages drives COVID-19 pathology. *Nature* **2022**, *606* (7914), 585–593.
(9) Lien, T. S.; Sun, D. S.; Chang, C. M.; Wu, C. Y.; Dai, M. S.; Chan, H.; Wu, W. S.; Su, S. H.; Lin, Y. Y.; Chang, H. H. Dengue virus and antiplatelet autoantibodies synergistically induce haemorrhage through Nlrp3-inflammasome and FcγRIII. *Thromb. Haemost.* **2015**, *113* (5), 1060–1070.
(10) Kim, H. W.; Canchola, J. G.; Brandt, C. D.; Pyles, G.; Chanock, R. M.; Jensen, K.; Parrott, R. H. Respiratory syncytial virus disease in infants despite prior administration of antigenic inactivated vaccine. *Am. J. Epidemiol.* **1969**, *89* (4), 422–434.
(11) Graham, B. S. Vaccines against respiratory syncytial virus: The time has finally come. *Vaccine* **2016**, *34* (30), 3535–3541.
(12) Polack, F. P. Atypical measles and enhanced respiratory syncytial virus disease (ERD) made simple. *Pediatr. Res.* **2007**, *62* (1), 111–115.
(13) Chakraborty, S.; Gonzalez, J.; Edwards, K.; Mallajosyula, V.; Buzzanco, A. S.; Sherwood, R.; Buffone, C.; Kathale, N.; Providenza, S.; Xie, M. M.; et al. Proinflammatory IgG Fc structures in patients with severe COVID-19. *Nat. Immunol.* **2021**, *22* (1), 67–73.
(14) Kolb, P.; Giese, S.; Voll, R. E.; Hengel, H.; Falcone, V. Immune complexes as culprits of immunopathology in severe COVID-19. *Med. Microbiol. Immunol.* **2023**, *212* (2), 185–191.
(15) Dejnirattisai, W.; Jumnainsong, A.; Onsirisakul, N.; Fitton, P.; Vasanawathana, S.; Limpitikul, W.; Puttikhunt, C.; Edwards, C.; Duangchinda, T.; Supasa, S.; et al. Cross-reacting antibodies enhance dengue virus infection in humans. *Science* **2010**, *328* (5979), 745–748.
(16) Sridhar, S.; Luedtke, A.; Langevin, E.; Zhu, M.; Bonaparte, M.; Machabert, T.; Savarino, S.; Zambrano, B.; Moureau, A.; Khromava, A.; et al. Effect of Dengue Serostatus on Dengue Vaccine Safety and Efficacy. *N. Engl. J. Med.* **2018**, *379* (4), 327–340.
(17) Wan, Y.; Shang, J.; Sun, S.; Tai, W.; Chen, J.; Geng, Q.; He, L.; Chen, Y.; Wu, J.; Shi, Z.; et al. Molecular Mechanism for Antibody-Dependent Enhancement of Coronavirus Entry. *J. Virol.* **2020**, *94* (5).
(18) Jaume, M.; Yip, M. S.; Cheung, C. Y.; Leung, H. L.; Li, P. H.; Kien, F.; Dutry, I.; Callendret, B.; Escriou, N.; Altmeyer, R.; et al. Anti-severe acute respiratory syndrome coronavirus spike antibodies trigger infection of human immune cells via a pH- and cysteine protease-independent FcγR pathway. *J. Virol.* **2011**, *85* (20), 10582–10597.
(19) Taylor, A.; Foo, S. S.; Bruzzone, R.; Dinh, L. V.; King, N. J.; Mahalingam, S. Fc receptors in antibody-dependent enhancement of viral infections. *Immunol. Rev.* **2015**, *268* (1), 340–364.
(20) Lučiūnaitė, A.; Mašalaitė, K.; Plikusiene, I.; Maciulis, V.; Juciute, S.; Norkienė, M.; Žvirblienė, A. Structural properties of immune complexes formed by viral antigens and specific antibodies shape the inflammatory response of macrophages. *Cell Biosci.* **2024**, *14* (1), 53.
(21) Xu, Z.; Shi, L.; Wang, Y.; Zhang, J.; Huang, L.; Zhang, C.; Liu, S.; Zhao, P.; Liu, H.; Zhu, L.; et al. Pathological findings of COVID-19 associated with acute respiratory distress syndrome. *Lancet Respir. Med.* **2020**, *8* (4), 420–422.
(22) Ankerhold, J.; Giese, S.; Kolb, P.; Maul-Pavicic, A.; Voll, R. E.; Göppert, N.; Ciminski, K.; Kreutz, C.; Lother, A.; Salzer, U.; et al. Circulating multimeric immune complexes contribute to immunopathology in COVID-19. *Nat. Commun.* **2022**, *13* (1), No. 5654.
(23) Larsen, M. D.; de Graaf, E. L.; Sonneveld, M. E.; Plomp, H. R.; Nouta, J.; Hoepel, W.; Chen, H. J.; Linty, F.; Visser, R.; Brinkhaus, M.; et al. Afucosylated IgG characterizes enveloped viral responses and correlates with COVID-19 severity. *Science* **2021**, *371* (6532), No. abc8378.
(24) Hoepel, W.; Chen, H. J.; Geyer, C. E.; Allahverdiyeva, S.; Manz, X. D.; de Taeye, S. W.; Aman, J.; Mes, L.; Steenhuis, M.; Griffith, G. R.; et al. High titers and low fucosylation of early human anti-SARS-CoV-2 IgG promote inflammation by alveolar macrophages. *Sci. Transl. Med.* **2021**, *13* (596), No. abf8654.
(25) Thulin, N. K.; Brewer, R. C.; Sherwood, R.; Bournazos, S.; Edwards, K. G.; Ramadoss, N. S.; Taubenberger, J. K.; Memoli, M.; Gentles, A. J.; Jagannathan, P.; et al. Maternal Anti-Dengue IgG Fucosylation Predicts Susceptibility to Dengue Disease in Infants. *Cell Rep.* **2020**, *31* (6), No. 107642.
(26) Ulrich, H.; Pillat, M. M.; Tárnok, A. Dengue Fever, COVID-19 (SARS-CoV-2), and Antibody-Dependent Enhancement (ADE): A Perspective. *Cytometry A* **2020**, *97* (7), 662–667.
(27) Pantaleo, G.; Correia, B.; Fenwick, C.; Joo, V. S.; Perez, L. Antibodies to combat viral infections: development strategies and progress. *Nat. Rev. Drug Discov.* **2022**, *21* (9), 676–696.
(28) Cecchinato, V.; Martini, V.; Pirani, E.; Ghovehoud, E.; Uguccioni, M. The chemokine landscape: one system multiple shades. *Front. Immunol.* **2023**, *14*, No. 1176619.
(29) Edgar, J. E.; Bournazos, S. Fc-FcγR interactions during infections: From neutralizing antibodies to antibody-dependent enhancement. *Immunol. Rev.* **2024**, *328* (1), 221–242.
(30) Crescioli, S.; Jatiani, S.; Moise, L. With great power, comes great responsibility: the importance of broadly measuring Fc-mediated

https://doi.org/10.1021/acsabm.6c00372
ACS Appl. Bio Mater. 2026, 9, 5196–5215

effector function early in the antibody development process. *MAbs* **2025**, *17* (1), No. 2453515.
(31) Nimmerjahn, F.; Ravetch, J. V. Fcgamma receptors as regulators of immune responses. *Nat. Rev. Immunol.* **2008**, *8* (1), 34–47.
(32) Mazor, Y.; Yang, C.; Borrok, M. J.; Ayriss, J.; Aherne, K.; Wu, H.; Dall'Acqua, W. F. Enhancement of Immune Effector Functions by Modulating IgG's Intrinsic Affinity for Target Antigen. *PLoS One* **2016**, *11* (6), No. e0157788.
(33) Kapcan, E.; Lake, B.; Yang, Z.; Zhang, A.; Miller, M. S.; Rullo, A. F. Covalent Stabilization of Antibody Recruitment Enhances Immune Recognition of Cancer Targets. *Biochemistry* **2021**, *60* (19), 1447–1458.
(34) Lux, A.; Yu, X.; Scanlan, C. N.; Nimmerjahn, F. Impact of immune complex size and glycosylation on IgG binding to human FcγRs. *J. Immunol.* **2013**, *190* (8), 4315–4323.
(35) Damelang, T.; Brinkhaus, M.; Osch, T. L. J.van; Schuurman, J.; Labrijn, A. F.; Rispens, T.; Vidarsson, G. Impact of structural modifications of IgG antibodies on effector functions. *Front. Immunol.* **2023**, *14*, No. 1304365.
(36) Li, D.; Edwards, R. J.; Manne, K.; Martinez, D. R.; Schäfer, A.; Alam, S. M.; Wiehe, K.; Lu, X.; Parks, R.; Sutherland, L. L.; et al. In vitro and in vivo functions of SARS-CoV-2 infection-enhancing and neutralizing antibodies. *Cell* **2021**, *184* (16), 4203–4219. e4232.
(37) Abduljaleel, Z.; Shahzad, N.; Aziz, S. A.; Malik, S. M. Monoclonal antibody designed for SARS-nCoV-2 spike protein of receptor binding domain on antigenic targeted epitopes for inhibition to prevent viral entry. *Mol. Divers.* **2023**, *27* (2), 695–708.
(38) Crowe, J. E. Human Antibodies for Viral Infections. *Annu. Rev. Immunol.* **2022**, *40*, 349–386.
(39) Arvin, A. M.; Fink, K.; Schmid, M. A.; Cathcart, A.; Spreafico, R.; Havenar-Daughton, C.; Lanzavecchia, A.; Corti, D.; Virgin, H. W. A perspective on potential antibody-dependent enhancement of SARS-CoV-2. *Nature* **2020**, *584* (7821), 353–363.
(40) Plikusiene, I.; Maciulis, V.; Juciute, S.; Ramanavicius, A.; Balevicius, Z.; Slibinskas, R.; Kucinskaite-Kodze, I.; Simanavicius, M.; Balevicius, S.; Ramanaviciene, A. Investigation of SARS-CoV-2 nucleocapsid protein interaction with a specific antibody by combined spectroscopic ellipsometry and quartz crystal microbalance with dissipation. *J. Colloid Interface Sci.* **2022**, *626*, 113–122.
(41) Chen, S.; Saeed, A. F. U. H.; Liu, Q.; Jiang, Q.; Xu, H.; Xiao, G. G.; Rao, L.; Duo, Y. Macrophages in immunoregulation and therapeutics. *Signal Transduct. Target. Ther.* **2023**, *8* (1), No. 207.
(42) Peckert-Maier, K.; Langguth, P.; Strack, A.; Stich, L.; Mühl-Zürbes, P.; Kuhnt, C.; Drassner, C.; Zinser, E.; Wrage, M.; Mattner, J.; et al. CD83 expressed by macrophages is an important immune checkpoint molecule for the resolution of inflammation. *Front. Immunol.* **2023**, *14*, No. 1085742.
(43) Ball, V.; Ramsden, J. Buffer dependence of refractive index increments of protein solutions. *Biopolymers* **1998**, *46* (7), 489–492.
(44) Höök, F.; Rodahl, M.; Kasemo, B.; Brzezinski, P. Structural changes in hemoglobin during adsorption to solid surfaces: effects of pH, ionic strength, and ligand binding. *Proc. Natl. Acad. Sci. U. S. A.* **1998**, *95* (21), 12271–12276.
(45) Lučiūnaitė, A.; McManus, R. M.; Jankunec, M.; Rácz, I.; Dansokho, C.; Dalgėdienė, I.; Schwartz, S.; Brosseron, F.; Heneka, M. T. Soluble Aβ oligomers and protofibrils induce NLRP3 inflammasome activation in microglia. *J. Neurochem.* **2020**, *155* (6), 650–661.
(46) Sinner, P.; Peckert-Maier, K.; Mohammadian, H.; Kuhnt, C.; Draßner, C.; Panagiotakopoulou, V.; Rauber, S.; Linnerbauer, M.; Haimon, Z.; Royzman, D.; et al. Microglial expression of CD83 governs cellular activation and restrains neuroinflammation in experimental autoimmune encephalomyelitis. *Nat. Commun.* **2023**, *14* (1), No. 4601.
(47) Bartneck, M.; Schrammen, P. L.; Möckel, D.; Govaere, O.; Liepelt, A.; Krenkel, O.; Ergen, C.; McCain, M. V.; Eulberg, D.; Luedde, T.; et al. The CCR2+ Macrophage Subset Promotes Pathogenic Angiogenesis for Tumor Vascularization in Fibrotic Livers. *Cell. Mol. Gastroenterol. Hepatol.* **2019**, *7* (2), 371–390.
(48) Huang, C.; Wang, Y.; Li, X.; Ren, L.; Zhao, J.; Hu, Y.; Zhang, L.; Fan, G.; Xu, J.; Gu, X.; et al. Clinical features of patients infected with 2019 novel coronavirus in Wuhan, China. *Lancet* **2020**, *395* (10223), 497–506.
(49) Lowery, S. A.; Sariol, A.; Perlman, S. Innate immune and inflammatory responses to SARS-CoV-2: Implications for COVID-19. *Cell Host Microbe* **2021**, *29* (7), 1052–1062.
(50) von Hundelshausen, P.; Agten, S. M.; Eckardt, V.; Blanchet, X.; Schmitt, M. M.; Ippel, H.; Neideck, C.; Bidzhekov, K.; Leberzammer, J.; Wichapong, K.; et al. Chemokine interactome mapping enables tailored intervention in acute and chronic inflammation. *Sci. Transl. Med.* **2017**, *9* (384).
(51) Boro, M.; Balaji, K. N. CXCL1 and CXCL2 Regulate NLRP3 Inflammasome Activation via G-Protein-Coupled Receptor CXCR2. *J. Immunol.* **2017**, *199* (5), 1660–1671.
(52) Blanco-Melo, D.; Nilsson-Payant, B. E.; Liu, W. C.; Uhl, S.; Hoagland, D.; Møller, R.; Jordan, T. X.; Oishi, K.; Panis, M.; Sachs, D.; et al. Imbalanced Host Response to SARS-CoV-2 Drives Development of COVID-19. *Cell* **2020**, *181* (5), 1036.
(53) Lee, S.; Channappanavar, R.; Kanneganti, T. D. Coronaviruses: Innate Immunity, Inflammasome Activation, Inflammatory Cell Death, and Cytokines. *Trends Immunol.* **2020**, *41* (12), 1083–1099.
(54) Rodrigues, T. S.; de Sá, K. S. G.; Ishimoto, A. Y.; Becerra, A.; Oliveira, S.; Almeida, L.; Gonçalves, A. V.; Perucello, D. B.; Andrade, W. A.; Castro, R.; et al. Inflammasomes are activated in response to SARS-CoV-2 infection and are associated with COVID-19 severity in patients. *J. Exp. Med.* **2021**, *218* (3).
(55) Zhang, J.; Wu, H.; Yao, X.; Zhang, D.; Zhou, Y.; Fu, B.; Wang, W.; Li, H.; Wang, Z.; Hu, Z.; et al. Pyroptotic macrophages stimulate the SARS-CoV-2-associated cytokine storm. *Cell. Mol. Immunol.* **2021**, *18* (5), 1305–1307.
(56) Pan, P.; Shen, M.; Yu, Z.; Ge, W.; Chen, K.; Tian, M.; Xiao, F.; Wang, Z.; Wang, J.; Jia, Y.; et al. SARS-CoV-2 N protein promotes NLRP3 inflammasome activation to induce hyperinflammation. *Nat. Commun.* **2021**, *12* (1), No. 4664.
(57) Yamin, R.; Jones, A. T.; Hoffmann, H. H.; Schäfer, A.; Kao, K. S.; Francis, R. L.; Sheahan, T. P.; Baric, R. S.; Rice, C. M.; Ravetch, J. V.; et al. Fc-engineered antibody therapeutics with improved anti-SARS-CoV-2 efficacy. *Nature* **2021**, *599* (7885), 465–470.
(58) Ruytinx, P.; Proost, P.; Van Damme, J.; Struyf, S. Chemokine-Induced Macrophage Polarization in Inflammatory Conditions. *Front. Immunol.* **2018**, *9*, No. 1930.
(59) Khalil, B. A.; Elemam, N. M.; Maghazachi, A. A. Chemokines and chemokine receptors during COVID-19 infection. *Comput. Struct. Biotechnol. J.* **2021**, *19*, 976–988.
(60) Li, X.; Mara, A. B.; Musial, S. C.; Kolling, F. W.; Gibbings, S. L.; Gerebtsov, N.; Jakubzick, C. V. Coordinated chemokine expression defines macrophage subsets across tissues. *Nat. Immunol.* **2024**, *25* (6), 1110–1122.
(61) Liechti, T.; Iftikhar, Y.; Mangino, M.; Beddall, M.; Goss, C. W.; O'Halloran, J. A.; Mudd, P. A.; Roederer, M. Immune phenotypes that are associated with subsequent COVID-19 severity inferred from post-recovery samples. *Nat. Commun.* **2022**, *13* (1), No. 7255.
(62) Bagheri, V.; Khorramdelazad, H.; Kafi, M.; Abbasifard, M. Chemokine CCL2 and its receptor CCR2 in different age groups of patients with COVID-19. *BMC Immunol.* **2024**, *25* (1), No. 72.
(63) Gutierrez-Chavez, C.; Aperrigue-Lira, S.; Ortiz-Saavedra, B.; Paz, I. Chemokine receptors in COVID-19 infection. *Int. Rev. Cell Mol. Biol.* **2024**, *388*, 53–94.
(64) Hachim, M. Y.; Hachim, I. Y.; Naeem, K. B.; Hannawi, H.; Al Salmi, I.; Hannawi, S. C-C chemokine receptor type 5 links COVID-19, rheumatoid arthritis, and Hydroxychloroquine: in silico analysis. *Transl. Med. Commun.* **2020**, *5* (1), 14.
(65) Kaivola, J.; Nyman, T. A.; Matikainen, S. Inflammasomes and SARS-CoV-2 Infection. *Viruses* **2021**, *13* (12), No. 2513.
(66) Del Valle, D. M.; Kim-Schulze, S.; Huang, H. H.; Beckmann, N. D.; Nirenberg, S.; Wang, B.; Lavin, Y.; Swartz, T. H.; Madduri, D.;

https://doi.org/10.1021/acsabm.6c00372
ACS Appl. Bio Mater. 2026, 9, 5196–5215

Stock, A.; et al. An inflammatory cytokine signature predicts COVID-19 severity and survival. *Nat. Med.* **2020**, *26* (10), 1636–1643.
(67) Lucas, C.; Wong, P.; Klein, J.; Castro, T. B. R.; Silva, J.; Sundaram, M.; Ellingson, M. K.; Mao, T.; Oh, J. E.; Israelow, B.; et al. Longitudinal analyses reveal immunological misfiring in severe COVID-19. *Nature* **2020**, *584* (7821), 463–469.
(68) Carty, M.; Guy, C.; Bowie, A. G. Detection of Viral Infections by Innate Immunity. *Biochem. Pharmacol.* **2021**, *183*, No. 114316.
(69) Deets, K. A.; Vance, R. E. Inflammasomes and adaptive immune responses. *Nat. Immunol.* **2021**, *22* (4), 412–422.
(70) Grosche, L.; Knippertz, I.; König, C.; Royzman, D.; Wild, A. B.; Zinser, E.; Sticht, H.; Muller, Y. A.; Steinkasserer, A.; Lechmann, M. The CD83 Molecule - An Important Immune Checkpoint. *Front. Immunol.* **2020**, *11*, No. 721.
(71) Brown, B.; Ojha, V.; Fricke, I.; Al-Sheboul, S. A.; Imarogbe, C.; Gravier, T.; Green, M.; Peterson, L.; Koutsaroff, I. P.; Demir, A.; et al. Innate and Adaptive Immunity during SARS-CoV-2 Infection: Biomolecular Cellular Markers and Mechanisms. *Vaccines (Basel)*. **2023**, *11* (2), No. 408.
(72) Julià, A.; Bonafonte-Pardàs, I.; Gómez, A.; López-Lasanta, M.; López-Corbeto, M.; Martínez-Mateu, S. H.; Lladós, J.; Rodríguez-Nunez, I.; Myers, R. M.; Marsal, S. Targeting of the CD80/86 proinflammatory axis as a therapeutic strategy to prevent severe COVID-19. *Sci. Rep.* **2021**, *11* (1), 11462.
(73) Langguth, P.; Peckert-Maier, K.; Beck, P.; Kuhnt, C.; Draßner, C.; Deinzer, A.; Steinkasserer, A.; Wild, A. B. CD83 acts as immediate early response gene in activated macrophages and exhibits specific intracellular trafficking properties. *Biochem. Biophys. Res. Commun.* **2023**, *647*, 37–46.
(74) Barozet, A.; Bianciotto, M.; Siméon, T.; Minoux, H.; Cortés, J. Conformational changes in antibody Fab fragments upon binding and their consequences on the performance of docking algorithms. *Immunol. Lett.* **2018**, *200*, 5–15.
(75) Al Qaraghuli, M. M.; Kubiak-Ossowska, K.; Ferro, V. A.; Mulheran, P. A. Antibody-protein binding and conformational changes: identifying allosteric signalling pathways to engineer a better effector response. *Sci. Rep.* **2020**, *10* (1), No. 13696.
(76) Kang, T. H.; Jung, S. T. Boosting therapeutic potency of antibodies by taming Fc domain functions. *Exp. Mol. Med.* **2019**, *51* (11), 1–9.
(77) Adachi, M.; Kurihara, Y.; Nojima, H.; Takeda-Shitaka, M.; Kamiya, K.; Umeyama, H. Interaction between the antigen and antibody is controlled by the constant domains: normal mode dynamics of the HEL-HyHEL-10 complex. *Protein Sci.* **2003**, *12* (10), 2125–2131.
(78) Tudor, D.; Yu, H.; Maupetit, J.; Drillet, A. S.; Bouceba, T.; Schwartz-Cornil, I.; Lopalco, L.; Tuffery, P.; Bomsel, M. Isotype modulates epitope specificity, affinity, and antiviral activities of anti-HIV-1 human broadly neutralizing 2F5 antibody. *Proc. Natl. Acad. Sci. U. S. A.* **2012**, *109* (31), 12680–12685.
(79) Wang, D.; Ye, J.; Hudson, S. D.; Scott, K. C.; Lin-Gibson, S. Effects of nanoparticle size and charge on interactions with self-assembled collagen. *J. Colloid Interface Sci.* **2014**, *417*, 244–249.

https://doi.org/10.1021/acsabm.6c00372
ACS Appl. Bio Mater. 2026, 9, 5196–5215